UNIVERSITY OF TURKU

# INVESTIGATION OF PROPERTIES OF SOLAR ENERGETIC PARTICLES AND GEOMAGNETIC STORMS RELATED TO CORONAL MASS EJECTIONS

Dheyaa Ameri

TURUN YLIOPISTON JULKAISUJA – ANNALES UNIVERSITATIS TURKUENSIS
SARJA - SER. AI OSA - TOM. 622 | ASTRONOMICA - CHEMICA - PHYSICA - MATHEMATICA | TURKU 2019

UNIVERSITY OF TURKU

# INVESTIGATION OF PROPERTIES OF SOLAR ENERGETIC PARTICLES AND GEOMAGNETIC STORMS RELATED TO CORONAL MASS EJECTIONS

Dheyaa Ameri

TURUN YLIOPISTON JULKAISUJA – ANNALES UNIVERSITATIS TURKUENSIS
SARJA - SER. AI OSA - TOM. 622 | ASTRONOMICA - CHEMICA - PHYSICA - MATHEMATICA | TURKU 2019

## University of Turku

Faculty of Science and Engineering
Department of Physics and Astronomy
Space Research Laboratory
Doctoral Programme in Physical and Chemical Sciences

## Research Director

Professor Rami Vainio
Department of Physics and Astronomy
University of Turku
Turku, Finland

## Supervised by

Research fellow Eino Valtonen
Department of Physics and Astronomy
University of Turku
Turku, Finland

Dr. Amjad Al-Sawad
Ministry of Higher Education and
Scientific Research
Baghdad, Iraq

## Reviewed by

Professor Raúl Gómez-Herrero
University of Alcala de Henares
Madrid, Spain

Dr. Monica Laurenza
National Institute of Astrophysics
Rome, Italy

## Opponent

Dr. Pertti Mäkelä
The Catholic University of America/NASA Goddard Space Flight Center
United States of America


The originality of this publication has been checked in accordance with the University of Turku quality assurance system using the Turnitin OriginalityCheck service.

ISBN 978-951-29-7913-4 (PRINT)
ISBN 978-951-29-7914-1 (PDF)
ISSN 0082-7002 (Print)
ISSN 2343-3175 (Online)
Painosalama Oy, Turku, Finland 2019

# Acknowledgments

All praise to Allah, glory and great, the almighty, the creator of universe, for giving me the blessing, the strength, the chance and endurance to complete this PhD thesis. O God, bless prophet Muhammad and his household.

First and foremost, I would like to express my sincere thanks to my supervisor Prof. Eino Valtonen for providing me an opportunity to complete my PhD thesis and related research. I appreciate his contributions of time and ideas to make my work productive and stimulating. His valuable suggestions, comments and guidance encourage me to learn more day by day. His deep insights helped me at various stages of my research. He gave me the tools and techniques of this science and I would never have been able to finish my dissertation without his guidance.

I wish to deeply thank my supervisor Dr. Amjad Al-Sawad for introducing me to this field of science and guiding me during my doctoral study. Without him I would have never known this field. I wish to thank my research director Prof. Rami Vainio for continuous support during my doctoral study.

I would like to express my thanks for scientific and administrative staff of the Department of Physics and Astronomy as they have provided the support and equipment that I needed to complete my thesis. I am grateful to Prof. Silja Pohjolainen for her great help in understanding the solar radio emissions that I needed in my research. I would also like to thank all my colleagues, including, but not limited to: Esa Riihonen and Osku Raukunen, who were willing to help me in various fields.

I gratefully acknowledge the funding sources that made my PhD work possible. This work was funded by the Ministry of Higher Education and Scientific Research of Iraq under grant 4552/2013.

Finally, I am grateful for my parents, who left this world. Without them I was not able to reach this far. I am grateful and thankful to my wife for the love, support, encouragement, and care she has always offered me. She has been a constant source of strength and inspiration to me especially in the moment when there was no one to answer my queries.

Turku, October 2019

*Dheyaa Ameri*

UNIVERSITY OF TURKU
Faculty of Science and Engineering
Department of Physics and Astronomy
Physics
DHEYAA AMERI: Investigation of Properties of Solar Energetic Particles and Geomagnetic Storms Related to Coronal Mass Ejections
Doctoral Dissertation, 145 pp.
Doctoral Programme in Physical and Chemical Sciences
October 2019

# ABSTRACT

Solar energetic particles (SEPs) and geomagnetic storms related to coronal mass ejections (CMEs) are a major research topic in solar-terrestrial and geospace physics. Solar energetic particles and coronal mass ejections can impact the Earth's ionosphere-magnetosphere-atmosphere system and lead to various adverse effects on space-born and ground-based technologies. This doctoral dissertation investigates the dependence of the properties of SEP events and geomagnetic storms on the parameters characterizing the CMEs and solar phenomena temporally related to the CMEs, such as solar flares and radio bursts.

We have carried out a statistical study of the properties of geomagnetic storms and SEP events associated with full-halo CMEs originating from close to the solar disk centre. We found that 50 % of all the selected CMEs were geoeffective and 39 % of these CMEs were associated with SEP events. We also investigated the dependence of the occurrence rate and strength of geomagnetic storms on the CME and solar flare parameters and on the solar wind conditions. This investigation covered the two most recent 11-year solar activity cycles and their different phases.

We have investigated the feasibility of using energetic particle and coronal mass ejection observations in geomagnetic storm forecasting. A good correlation was found between the storm strength and three parameters, two of them characterizing the solar proton events and one the direction of the CMEs. We proposed an empirical equation based on these three parameters to be used for mid-term forecasting of geomagnetic storm strengths enabling warning times of $(15 \pm 10)$ hours.

In a comprehensive analysis of high-energy solar proton events we discovered that these events can be divided into two categories based on the associations of the proton events and on the proton release times with respect to the temporally related radio type II bursts. Category 1 proton events were related to metric type II bursts, while in Category 2 the proton events were associated with decametric-hectometric type II emission. The events in Categories 1 and 2 exhibited significantly different characteristics due to acceleration in different heights in the solar atmosphere and possibly in different processes.

KEYWORDS: Solar Energetic Particles, Geomagnetic Storms, Coronal Mass Ejections, Solar Flares, Radio Bursts.

TURUN YLIOPISTO
Luonnontieteiden ja tekniikan tiedekunta
Fysiikan ja tähtitieteen laitos
Fysiikka
DHEYAA AMERI: Auringon koronan massapurkauksissa syntyvät suurienergiaiset hiukkaset ja geomagneettiset myrskyt
Väitöskirja, 145 s.
Fysikaalisten ja kemiallisten tieteiden tohtoriohjelma
Lokakuu 2019

# TIIVISTELMÄ

Auringon koronan massapurkausten suurienergiaiset hiukkaset ja massapurkausten aiheuttamat geomagneettiset myrskyt ovat Aurinko-Maa-fysiikan ja Maan lähiavaruuden fysiikan merkittäviä tutkimuskohteita. Suurienergiaiset hiukkaset ja massapurkaukset voivat vaikuttaa Maan ionosfääriin, magnetosfääriin ja ilmakehään ja aiheuttaa haitallisia ilmiöitä sekä avaruudessa että Maan pinnalla käytettävissä teknisissä järjestelmissä. Väitöskirjassa tutkitaan Auringon suurienergiaisten hiukkasten ja geomagneettisten myrskyjen riippuvuutta massapurkausten ja Auringon soihtujen ja radiopurkausten ominaisuuksista.

Auringon kiekon keskiosan ja koronagrafikuvissa koko Auringon kiekon peittävistä massapurkauksista puolet todettiin geoefektiivisiksi eli aiheuttavan geomagneettisen myrskyn ja lähes puoleen näistä purkauksista liittyi suurienergiaisten hiukkasten intensiteetin voimakas kasvu. Geomagneettisten myrskyjen esiintymistiheyden ja voimakkuuden havaittiin riippuvan Auringon massapurkausten ja soihtujen ominaisuuksista. Tutkimus kattoi kaksi Auringon 11-vuotista jaksoa ja jaksojen eri vaiheet.

Väitöskirjassa tutkittiin Auringon hiukkasten ja massapurkausten havainnoinnin hyödyllisyyttä geomagneettisten myrskyjen ennustamisessa. Havaittuun hiukkasvuohon liittyviin kahteen ominaisuuteen ja massapurkauksen kulkusuuntaa kuvaavaan parametriin perustuen kehitettiin kokeellinen malli, jonka avulla myrskyn voimakkuus pystyttiin ennakoimaan. Menetelmää voidaan käyttää keskipitkän ajan ennusteessa, jonka varoitusajan havainnoista myrskyn alkamiseen todettiin olevan ($15\pm10$) tuntia.

Laajaan Auringon suurienergiaisten hiukkasten analyysiin perustuen todettiin voitavan jakaa hiukkaspurkaukset kahteen ryhmään riippuen purkausten alkamisen ajallisesta suhteesta Auringon tyypin II radiopurkauksiin. Ryhmän 1 hiukkaspurkaukset liittyivät tyypin II radiopurkauksiin metrin aallonpituusalueella, kun taas ryhmän kaksi tapauksiin liittyi radiopurkaus dekametri-hehtometri -aallonpituusalueella. Eri ryhmiin kuuluvien hiukkastapausten ominaisuudet poikkesivat merkittävästi toisistaan. Eron selitti hiukkasten kiihdytys eri korkeuksissa Auringon koronassa ja mahdollisesti toisistaan poikkeavat kiihdytysmenetelmät.

ASIASANAT: Auringon suurienergiaiset hiukkaset, Geomagneettiset myrskyt, Koronan massapurkaukset, Auringon soihdut, Radiopurkaukset.

# List of Original Publications

This thesis is research work in data analysis of space weather events carried out at the Space Research Laboratory, Department of Physics and Astronomy, University of Turku during the years 2014 – 2019. The thesis consists of an introductory part and the following four original publications.

**I. Investigation of the Geoeffectiveness of Disk-Centre Full-Halo Coronal Mass Ejections.**
Dheyaa Ameri and Eino Valtonen.
Solar Physics, **Vol.292**, 79, (2017).

**II. Potential Role of Energetic Particle Observations in Geomagnetic Storm Forecasting.**
Dheyaa Ameri and Eino Valtonen.
Advances in Space Research, **Vol.64**, 801, (2019).

**III. Solar Energetic Particle Events Related to Disk-Centre Full-Halo Coronal Mass Ejections.**
Eino Valtonen and Dheyaa Ameri.
Proceedings of the 34th International Cosmic Ray Conference, PoS (ICRC2015) **87** (2015).

**IV. Properties of High-Energy Solar Particle Events Associated with Solar Radio Emissions.**
Dheyaa Ameri, Eino Valtonen, and Silja Pohjolainen.
Solar Physics, **Vol.294**, 122, (2019).

The original publications have been reproduced with the permission of the copyright holders.

# Contents

# Abbreviations

| | |
|---|---|
| AU | Astronomical Unit |
| $B_s$ | Southward Component of the Magnetic Field |
| $B_t$ | Total Magnetic Field Strength |
| CELIAS | Charge, Element, and Isotope Analysis System (on board SOHO) |
| CME | Coronal Mass Ejection |
| DC-FH-CME | Disk Centre Full Halo Coronal Mass Ejection |
| DH | Decametric-Hectometric |
| DP | Direction Parameter |
| Dst | Disturbance Storm Time |
| 3DP | 3-D Plasma and Energetic Particle Investigation (on board Wind) |
| $E_y$ | Y-component of the Solar Wind Electric Field |
| EM | Electromagnetic |
| EPS | Energetic Particle Sensor (on board GOES) |
| ERNE | Energetic and Relativistic Nuclei and Electrons (on board SOHO) |
| ESP | Energetic Storm Particle |
| EUV | Extreme UltraViolet |
| GIC | Geomagnetically Induced Current |
| GOES | Geostationary Operational Environment Satellite |
| $H_\alpha$ | Spectral Line of hydrogen at a wavelength of 656.3 nm |
| HED | High Energy Detector (detector telescope in ERNE) |
| HEPAD | High energy Proton and Alpha Detector (on board GOES) |
| HSS | High-speed Stream |
| ICME | Interplanetary Coronal Mass Ejection |
| IMF | Interplanetary Magnetic Field |
| IP | Interplanetary |
| ISEE-3 | The third of three International Sun-Earth Explorers |
| $K_p$ | Global Geomagnetic Activity Index |
| L1 | First-Lagrangian point |
| LASCO | Large Angle Spectrometric Coronagraph (on board SOHO) |
| LED | Low Energy Detector (detector telescope in ERNE) |
| m | metric (radio emission) |
| m-km | metric to kilometric (radio emission) |
| OMNI | Database of the space physics data facility |
| OSO-7 | 7th Orbiting Solar Observatory |
| $R_\odot$ | Solar Radius |
| RL | Radio-Loud |
| RQ | Radio-Quiet |
| SC | Solar Cycle |
| SEP | Solar Energetic Particle |
| SMM | Solar Maximum Mission |

| | |
|---|---|
| SOHO | Solar and Heliospheric Observatory (ESA/NASA satellite) |
| STEREO | Solar Terrestrial Relations Observatory (NASA satellite) |
| UV | Ultraviolet |
| $V_{sw}$ | Solar Wind Speed |
| WAVES | Radio and Plasma Wave Experiment (on board Wind) |
| Wind | NASA's Satellite |

# Chapter 1

# Introduction

## 1.1 Sun and Space Weather

### 1.1.1 General Description of the Sun

The Sun is the nearest star to our Earth and our solar system is located in the Milky Way Galaxy. The Sun is a gigantic sphere of ionized gas with a radius of $6.96 \times 10^5$ km (109 Earth radii), a volume of $1.41 \times 10^{24}$ km$^3$ (1.3 million Earths), and a mass of $1.99 \times 10^{30}$ kg ($> 99$ % of the solar system mass). The chemical composition of the Sun is 92.1 % hydrogen, 7.8 % helium, and 0.1 % all other ions. The temperature ranges from $15.6 \times 10^7$ K at the Sun's centre to 5780 K on the surface. The solar luminosity is $3.85 \times 10^{26}$ W which leads to the solar constant of 1366 W m$^{-2}$ at 1 AU. The solar rotation period is about 25 days at the equator and 35 days close to the poles. The age of the Sun is about $4.6 \times 10^9$ years.

### 1.1.2 Solar Structure

The Sun can be divided in six layers. From the centre outwards, the layers of the Sun are: the solar interior composing of the core, the radiative zone, and the convective zone, the visible surface known as the photosphere, the chromosphere, and finally the outermost layer, the corona.

The Sun's energy is liberated in nuclear fusion reactions. Hydrogen is transformed to helium in the Sun's core. According to Einstein's theory, the mass differences between four hydrogen nuclei and one helium nucleus is converted into a vast quantity of energy which is released in the form of photons and kinetic energy. The energy diffuses outward through the inner spherical shell of the radiative zone in the form of photons, until reaching the outer spherical shell of the convective zone. At the Sun's surface the visible activity begins.

### 1.1.3 Solar Surface Phenomena

Processes and structures occurring on the visible surface of the Sun include the following: *Granulation* is seen as bright irregular formations surrounded by darker lanes that cover the photosphere. They are believed to be hot plasma regions that rise to the top of the convection zone. Once they cool, the edges turn dark and the plasma sinks back into

the convection zone. *Sunspots* are dark areas on the photosphere that are much cooler than their surroundings. They occur in regions of the Sun which have strong magnetic fields, and appear in pairs with opposite magnetic polarity. The sunspots appear and disappear, rising from inside the Sun and moving back into it. They remain visible from a few hours to weeks and even months. Sunspot groups are associated with large active regions which are responsible for most of the Sun's observable activity. *Faculae* are bright structures (in white light) on the photosphere associated with active regions. They are brighter, hotter, and denser than their surroundings. They can occur before sunspots appear and can remain in place for several months after the sunspots have disappeared. They are associated with areas of higher magnetic fields, but these fields are not as strong as those associated with sunspots.

*Plages* are bright regions (in $H_\alpha$ and Ca II lines) floating in the chromosphere above active regions in the photosphere. They are brighter, hotter, and denser than their surroundings, and are caused by the magnetic fields of active regions. *Filaments (prominences)* are massive loops of chromospheric cool dense gas that arch up above the photosphere. Seen from above, they appear dark because the gas inside is cool compared to the hot photosphere below. But seen in profile against the dark sky they look like giant glowing loops, and are then called prominences.

*Flares* are sudden and intense eruptions in the low corona that often accompany sunspots. Flares radiate at many frequencies, from X-rays and gamma rays to long wavelength radio waves. They also emit high energy particles, sometimes called solar cosmic rays, including protons, electrons, and heavier nuclei. *Coronal holes* are dark regions seen in the corona in extreme ultraviolet and soft X-ray images. They are darker, cooler, and less dense regions than the surrounding plasma. They are regions of open unipolar magnetic fields which allow the solar wind to escape into space, resulting in streams of fast solar wind. *Coronal Mass Ejections (CMEs)* are large expulsions of plasma and magnetic field from the corona. CMEs travel outward from the Sun at speeds ranging from slower than 250 km $s^{-1}$ to as fast as near 3000 km $s^{-1}$. The fastest Earth-directed CMEs can reach our planet in as little as 15-18 hours, while slower CMEs can take about 2 – 4 days to arrive.

Figure 1.1 shows the most significant solar phenomena observed at different wavelengths. The left top panel of Figure 1.1 is a Solar Terrestrial Relations Observatory (STEREO) image on June 27, 2011 in extreme ultraviolet showing three major magnetic solar features: a coronal hole, an active region, and a long filament. Sunspots near solar maximum on September 27, 2001 from the Solar and Heliospheric Observatory (SOHO) spacecraft are presented in the right top panel. The left and right bottom panels of Figure 1.1, also from SOHO, show two major solar phenomena: a solar flare and a CME, respectively.

### 1.1.4 Magnetic Activity Cycle of the Sun

The solar dynamo is the source of the Sun's magnetism. The solar dynamo amplifies and regenerates the Sun's magnetic field within the solar interior. The hot circulating gases, which are good conductors of electricity, generate electrical currents that create

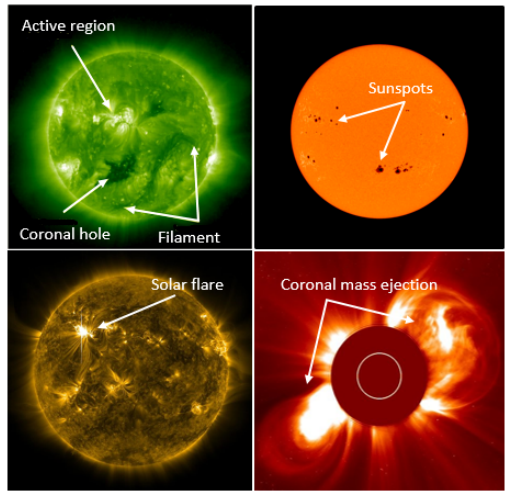


Figure 1.1: Significant solar phenomena observed at different wavelengths.

magnetic fields. These fields in turn sustain the generation of electricity. The process of field amplification is cumulative, so an intense magnetic field can be generate from an initially weak one. These strong fields eventually rise through the convective zone and emerge at the photosphere (Lang, 2001).

There are two different magnetic zones in the solar corona that have fundamentally different properties: open-field and closed-field regions. Open-field regions, which always exist in the polar regions and sometimes extend towards the equator, connect the solar surface with the interplanetary field and are the source of the fast solar wind ($\sim$800 km s$^{-1}$). Closed-field regions, which always exist in the solar equator and can extend towards regions close to the poles, contain mostly closed field lines in the corona up to heights of about one solar radius. At higher altitudes the closed field lines open up and connect eventually to the heliosphere, and produce a slow solar wind component (speed $\sim$400 km s$^{-1}$). Closed-field regions contain all the bright and overdense coronal loops, produced by filling with chromospheric plasma that stays trapped in these closed field lines. The magnetic field on the solar surface is very inhomogeneous. The strongest magnetic field regions are in sunspots with field strengths in the range of $\sim 0.2-0.3$ T, while active regions and their plages comprise a larger area around sunspots with typical fields of $\sim 0.1$ T.

The solar activity varies with a period of about 11 years, and is seen as a corresponding periodic variation of the total number of sunspots. The sunspot cycle was first noted by Samuel Heinrich Schwabe (1840). The number of sunspots varies from a minimum at the beginning of the 11-year cycle to a maximum at the mid-cycle and back to a minimum at the end of the cycle. The magnetic field of the Sun at the time of maximum activity is disordered, but stronger than at minimum. Most of the solar activities are magnetic in origin and easily-observed. The sunspot cycle is also referred to as the magnetic activity cycle of the Sun. The rates of solar explosions, including powerful flares and CMEs, also follow this 11-year cycle. The properties of sunspots

and the associated active regions vary during the solar cycle. During the cycle minimum the solar magnetic field has a form of a dipole field extending from pole to pole. During the cycle maximum, the magnetic field is more disordered, and the bipolar sunspot groups are created when the magnetic loops break through the photosphere. The active regions are formed in two belts relatively near to the equator in the northern and southern hemisphere.

### 1.1.5 Solar Wind

Solar wind is a continuous flow of charged particles (plasma) released from the Sun. The solar wind flows out with an average speed of about 470 $\mathrm{km\,s^{-1}}$ and has an average density of about 5 $\mathrm{cm^{-3}}$ at 1 AU. Both the speed and the density are variable with a 5 – 95 % range of cumulative probability of occurrence of 320 – 710 $\mathrm{km\,s^{-1}}$ and 3.2 – 20 $\mathrm{cm^{-3}}$, respectively (ECSS, 2008). The solar wind can be classified in two types: slow solar wind from the equatorial regions of the Sun, and fast solar wind originating from coronal holes, usually located in the polar regions of the Sun. When a high-speed solar wind overtakes slow-speed wind, it creates something known as a corotating interaction region. These interaction regions consist of solar wind with very high densities and strong magnetic fields (Tsurutaini & Gonzalez, 1997). Since the Sun's magnetic field is embedded in the plasma, the solar wind carries with it a magnetic field of about 5 nT. The magnetic field in interplanetary (IP) space has a wavy structure, which leads to a current sheet-separated sector structure with the magnetic field direction alternately towards and away from the Sun (Russell, 2001). The solar wind speed, the solar wind density, and the strength and direction of the magnetic field embedded in the solar wind are important sources for space weather impacts on Earth.

## 1.2 Space Weather

### 1.2.1 Definition of Space Weather

Space weather refers to the time-variable conditions in the space environment, including the conditions on the Sun and in the interplanetary space, and in the Earth's magnetosphere, ionosphere and thermosphere, that can affect the performance of space-borne and ground-based technological systems and can endanger human life or health (e.g. Pirjola , 2007).

Due to the continued development in technological systems, the importance of space weather is continuously increasing as society becomes more dependent on reliable technology. Space weather risks have become significantly influential and play important role in the design of many technological systems, in particular spacecraft.

### 1.2.2 Sources of Space Weather Effects

The Sun is the ultimate source of most of the space weather effects. Solar flares, coronal mass ejections, and coronal holes represent the significant solar phenomena leading to space weather events. These solar phenomena are responsible for various dis-

turbances propagating in interplanetary space. The most significant manifestations of space weather are the following (e.g. Bothmer & Zhukov, 2007; Valtonen, 2004, and references therein).

*Space plasmas* are continuously emanating from the Sun and propagating into interplanetary space in the form of solar wind. The solar wind consists mainly of protons ($\sim 95\,\%$) with small portions of electrons, helium ions, and heavy ions. During solar disturbances, the speed and density of the solar wind is highly variable.

*Particle radiation*, which in general consists of protons and electrons and small amounts of helium ions and heavy ions, includes three main components: galactic cosmic rays (GCRs), solar energetic particles (SEPs), and trapped radiation. GCRs originate from outside of the solar system and are characterized by low intensities and high energies. SEPs are accelerated at the Sun or in the IP medium during solar eruptions, and propagate along IP magnetic field lines from the Sun to the Earth. SEPs are the major source of high-energy particles during the maximum of the solar activity cycle. During solar explosions, sudden highly enhanced fluxes of SEPs can reach the Earth within a few tens of minutes. Trapped particles appear in the radiation belts encircling the Earth. The radiation belts are usually divided into the inner belt which is dominated by protons, and the outer belt dominated by electrons.

*Interplanetary magnetic field* (IMF) represents the Sun's magnetic field carried out by the solar wind. During solar disturbances, the direction and strength of the IMF is highly variable and significantly affects the geomagnetic activity.

*Electromagnetic radiation* is emitted from the Sun. The wavelengths range from $\gamma$ rays to radio waves. The fluxes of ultraviolet, X-rays, and radio bursts related to solar explosions are highly variable over the 11-year solar cycle.

### 1.2.3 Space Weather Consequences

Space weather effects arise from the highly variable conditions in the geospace environment due to the solar activity and lead to various energetic effects in the Earth's magnetosphere–ionosphere system and on the ground. These effects in turn affect many technological systems.

#### Space Weather Effects on Spacecraft Systems and Operations

The modern spacecraft systems appear to be increasingly vulnerable to space environment. This is probably due to softer designs of electronic components and reduction in subsystem sizes and other reasons (Baker, 2000). The space environment consists of various complex phenomena which can have strong effects on the spacecraft operation in different aspects. Most significant effects on spacecraft and satellites caused by the space environment are the following (e.g. Daly et al., 2007; Valtonen, 2004; Lu et al., 2019, and references therein):

*Surface charging* is the process of electric charge accumulation on surfaces exposed to space environment and is considered as the most significant effect on spacecraft leading to mission failures. It is produced by the interaction between the surface and the

ambient plasma. The surface charging of spacecraft systems can result in surface discharges (e.g. Estienne, 1993), causing surface damage and degradation, and in some cases operational anomalies and failures. The enhanced fluxes of energetic particles produced by the large solar flares and CMEs between mid-October and early November 2003 led to anomalies on many spacecraft (e.g. Barbieri & Mahmot, 2004).

*Internal charging* is the buildup of electric charge, caused by the accelerated electrons, inside the spacecraft when impinging charged particles have sufficient energies to penetrate in the dielectric materials used in the subsystems. Internal charging of spacecraft systems results in bulk discharge and can present a direct hazard to electronics (e.g. Estienne, 1993).

*Ionizing dose* is the deposition of energy by a charged particle, including trapped protons and electrons, in a matter by ionization, occurring when energetic particles pass through the matter. The integral of the particle flux and the ionization energy loss rate gives the total ionizing dose. The effects of the total ionizing dose include changes in the static and dynamic response of an electronic component possibly causing a complete functional failure of the component.

*Non-ionizing dose* refers to the kinetic energy transferred in the interactions of incident particles, including protons and electrons, to entire atoms of the medium without causing ionization of the medium. A long-term cumulative effect with increased lattice defect density is known as displacement damage. It is the main degradation mechanism in space for certain semiconductor devices, such as solar cells and charge-coupled devices.

*Single event effects* are instantaneous electrical disturbances that disrupt the normal operation of microelectronics circuits, and are caused by a single charged particle losing energy by ionization in a sensitive device. High-energy heavy ions are important sources of single event effects. The effects can be classified into two categories: soft errors, which are non-destructive, and hard errors, which are potentially destructive and cause permanent functional effects (Dodd & Massengill, 2003).

### Space Weather Effects on Communications

Solar-terrestrial phenomena can affect the communications systems. These effects have been discovered from the earliest telegraph systems to modern wireless communications using satellites and land links. Modern communications technologies can be affected by the solar-terrestrial environment in various ways (e.g. Lanzerotti, 2007, and references therein).

*Ionosphere variation:* Solar storms can change the Earth's ionosphere affecting the signal propagation, reflection, and attenuation. During a geomagnetic storm, the Earth's magnetosphere-ionosphere becomes highly disturbed, containing intense and rapidly-varying currents. The varying currents can cause considerable problems at all geomagnetic latitudes affecting navigation signals from the Earth-orbiting Global Positioning System. The changes in the geomagnetic field can cause inducted electrical currents in the Earth that in turn affect the cable communication systems.

*Solar radio bursts:* Solar radio emissions can cause considerable excess noise in

wireless communications systems and interference with radar and radio receivers. In an analysis of the potential problems in a wireless cell site caused by solar radio bursts, Bala et al. (2002) found that the occurrence rate of the potential problems was on average once every three to four days during solar maximum, and perhaps once every twenty days or less during solar minimum.

*Magnetic field variations:* During large solar wind disturbances, the large variation of the magnetic fields that occur at the boundary and outside the magnetosphere can seriously disrupt the stabilisation of any geosynchronous communication satellite which uses the Earth's magnetic field for attitude control.

### Space Weather Effects on Power Transmission Systems

One of the direct effects of space weather are the geomagnetic storms. During a geomagnetic storm driven by the solar activity, the changes in the geoelectric field produce currents, known as geomagnetically induced currents (GIC), in ground-based power transmission networks such as power grids, oil and gas pipelines. GIC can cause different kinds of damage in the power transmission systems (Pirjola , 2007, and references therein). Two most famous and serious GIC events that led to power grid collapse were the Hydro-Quebec blackout in Canada in March 1989 (e.g. Bolduc, 2002) and a blackout in Sweden in October 2003 (e.g. Wik et al., 2008).

# Chapter 2

# Coronal Mass Ejections and Solar Flares

## 2.1 Coronal Mass Ejections

Coronal mass ejections are expulsions of coronal plasma and magnetic field entrained therein into the heliosphere. They were first observed by using the white-light coronagraph on board the NASA's $7^{th}$ Orbiting Solar Observatory (OSO-7) and Skylab at the beginning of the 1970s (e.g. Gosling, 1997). Gosling et al. (1974) described the general characteristics of CMEs. Since OSO-7 and Skylab observations, thousands of CMEs have been identified using data from the U.S. Air Force P78-1 satellite (1979 – 1985), NASA's Solar Maximum Mission (SMM, 1980 and 1984 – 1989), and the Large Angle Spectrometric Coronagraph (LASCO) on the SOHO spacecraft (1996 – current). LASCO observes the corona from 1.1 to 30 solar radii from the Sun centre, looking closer to, and further from, the Sun than all previous space-borne coronagraphs. More recently (2006), the NASA's Solar Terrestrial Relations Observatory (STEREO) mission was launched to study the 3D nature of CMEs, their initiation and propagation in interplanetary space. The prototypical CME was identified by Illing & Hundhausen (1983) who showed that the CME often exhibits a three-part structure in which the front is followed by a cavity of reduced density and a bright core (see Figure 2.1c).

### 2.1.1 Characteristics of CMEs

Many studies based on the observations obtained from different satellites have established the essential characteristics of CMEs close to the Sun (e.g. Howard et al., 1985; Hundhausen, 1993, 1994; Kahler, 2006; Gopalswamy, 2004b, 2006a; Gopalswamy et al., 2009; Gopalswamy, 2010b). The occurrence rate of CMEs during the solar activity cycle varies by more than an order of magnitude. The daily CME rate averaged over the Carrington rotation periods ranges from $< 0.5$ during the solar minimum to $> 6$ during the solar maximum. A high correlation between the CME rate and the sunspot number was found for solar cycle 23, but it was not uniform throughout the cycle. The correlation was high during the rise ($\sim$0.90) and declining ($\sim$0.73) phases, but was lower during the maximum phase ($\sim$0.64). The low correlation during the maximum phase has been attributed to CMEs originating from non-spot regions. The average of the

ejection masses is in the range of $10^9 - 10^{13}$ kg with a median value of $\sim 3.2 \times 10^{11}$ kg. The leading edge speeds range from $< 20\,\mathrm{km\,s^{-1}}$ to $> 3000\,\mathrm{km\,s^{-1}}$ with an average of $466\,\mathrm{km\,s^{-1}}$. CMEs are characterized by the angular width which is measured as the position angle extent of the CMEs in the sky plane seen in the coronagraph images. The angular width is in the range of $\sim 5^\circ - 360^\circ$ with an average value of $41^\circ$. Using the speed and mass measurements, the kinetic energy can be computed and ranges from $\sim 10^{19}$ J to $\sim 10^{26}$ J with an average $\sim 2 \times 10^{22}$ J (Gopalswamy, 2010b, and references therein).

Different studies have emphasized that CMEs may be associated with solar flares (Rust et al., 1980), filament (prominence) eruptions (Gosling et al., 1974; Sheeley et al., 1975), streamers (Howard et al., 1985), soft X-rays, radio bursts, shocks (Sheeley et al., 1983, 1984, 1985), and solar energetic particles (Kahler et al., 1985). Sheeley et al. (1999) have suggested that CMEs can be distinguished into two dynamical classes, gradual and impulsive (see also, Moon et al., 2002; Zhang et al., 2002; Zhang & Golub, 2003). The gradual CMEs are slower and accelerate in the coronagraph field of view, and are associated with prominence eruptions, while the impulsive CMEs are faster and decelerate in the coronagraph field of view, and are associated with solar flares. The investigation of Vršnak et al. (2005), however, contradicted this distinct division.

Based on the observations of the LASCO white-light coronagraphs, CMEs have often been divided into three angular width groups, narrow (angular width $< 20^\circ$), normal ($20^\circ$ to $120^\circ$), and halo ($\geq 120^\circ$). Halo CMEs can be full ($360^\circ$) or partial ($\geq 120^\circ$) (see Figure 2.1). The portions of the three angular width groups are: narrow, $\sim$18 %; normal, $\sim$70 %; and halo $\sim$12 % (Gopalswamy, 2004b). The slow CMEs ($\leq 250\,\mathrm{km\,s^{-1}}$) show acceleration, intermediate speed CMEs (from $250\,\mathrm{km\,s^{-1}}$ to $450\,\mathrm{km\,s^{-1}}$) have little acceleration, and most of the fast CMEs ($> 450\,\mathrm{km\,s^{-1}}$) show deceleration in the coronagraph field of view (Yashiro et al., 2004). The average speed of halo CMEs ($\sim 1000\,\mathrm{km\,s^{-1}}$) is more than twice that of the normal CMEs ($\sim 450\,\mathrm{km\,s^{-1}}$) (e.g. Yashiro et al., 2004; Gopalswamy, 2004b). The halo CMEs typically originate from close to the disk centre and propagate into interplanetary space, either towards or away from the Earth (e.g. Burkepile et al., 2004). Those propagating towards the Earth are often associated with shocks, SEPs, and geomagnetic storms at Earth. Halo CMEs are considered as a more energetic CME group than the narrow CMEs (e.g. Michałek et al., 2003; Gopalswamy, 2004b). Most full halo CMEs are faster than $900\,\mathrm{km\,s^{-1}}$, have a high ability in driving shocks and producing SEPs (Kahler & Reames, 2003).

### 2.1.2 CME Models

Several models have been presented describing the physical mechanisms of CME initiation either analytically or by numerical simulations. Various CME models explain these solar eruptions in different details, but they all agree that a CME is the result of a catastrophic loss of mechanical equilibrium of solar plasma confined by the coronal magnetic field. Based on the assumed state of the coronal magnetic field, the CME models can be organized in two main groups (Roussev & Sokolov, 2006): flux rope models and sheared-arcade models.

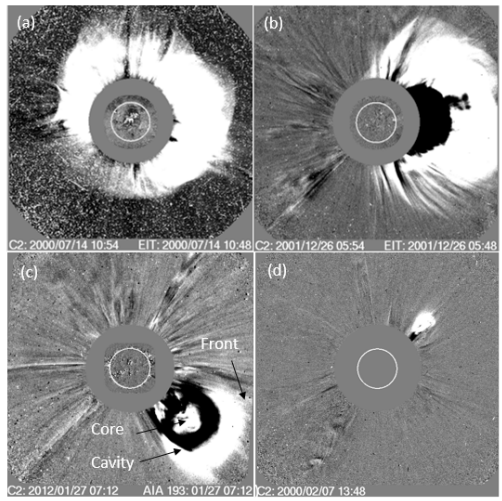


Figure 2.1: White-light coronagraph images of SOHO/LASCO showing CMEs with different angular widths. Panels a, b, c, and d show a full halo, partial halo, normal, and narrow CME, respectively.

*Flux rope models* assume that a twisted magnetic flux rope exists prior to the eruption. The flux rope is suspended in the solar corona by the balance between magnetic compression, hoop, and tension forces associated with the magnetic field of the rope and the background field. The mechanical equilibrium in flux-rope models is dependent on the gravity and pressure gradient forces. This model suggests that flux ropes may suddenly lose mechanical equilibrium and erupt due to footpoint motions, or by injection of magnetic helicity. In case the flux rope includes a prominence, the eruption can be triggered via some active instability mechanism in which most of the prominence mass has been drained through the footpoints of the flux rope.

*Sheared-arcade models* assume that the flux rope is formed in the course of the eruption. In these models, the sheared magnetic arcades contain the free energy in the form of electric current and the sudden loss of equilibrium of the coronal magnetic field and a subsequent eruption is achieved by magnetohydrodynamic processes (i.e. magnetic reconnection). The magnetic reconnection is the fundamental trigger of the eruption. Sheared-arcade models can also be divided in three subclasses depending on the height at which the magnetic reconnection occurs. The three subclasses are the following:

*Flux-cancellation model* (e.g. Roussev et al., 2004) assumes that the magnetic reconnection can occur at the photosphere or near the base of the corona. The slow reconnection (i.e., cancellation process) leads to the formation of a flux rope, which increases in both size and twist with time. The outward force associated with this twist strengthens until eventually the overlying field is no longer able to confine the rope. The dynamics of the eruption proceed in the same manner as in the flux-rope models.

In the *tether-cutting model*, proposed by Moore et al. (2001), the magnetic recon-

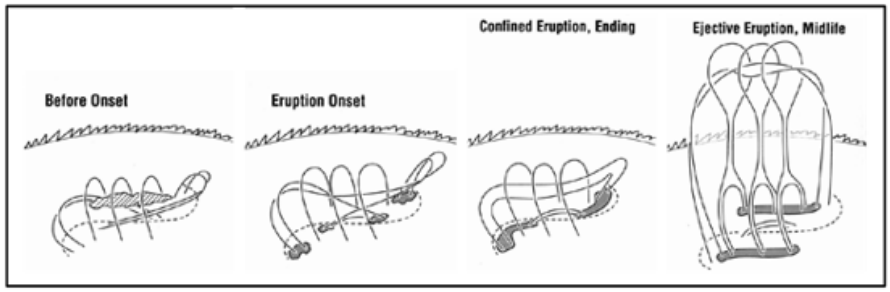


Figure 2.2: The configuration of the tether-cutting model. The figure is reproduced from Moore et al. (2001). The dashed curve is the photospheric neutral line. The ragged arc in the background is the chromospheric limb. The gray areas are bright patches or ribbons of flare emission in the chromosphere at the feet of reconnected field lines. The diagonally lined feature above the neutral line in the first panel is the filament.

nection can occur inside the coronal filament in the low corona. Some observational phenomena, such as the brightenings in multi-wavebands (e.g. Yurchyshyn et al., 2006), slow-rise motion of filaments (e.g. Sterling et al., 2011) and morphological changes of flaring structures (e.g. Cheng et al., 2014) have supported the tether-cutting model. In this model, the reconnection process occurs when the filaments, which are comprised of a number of magnetic threads of opposite polarity, collide or merge with each other during their eruption. In this process, all connections of the filaments (tethers) with the photosphere are cut, except for those at the ends of the erupting flux rope. The configuration of this model presented by Moore et al. (2001) is shown in Figure 2.2. There are two possibilities for how the explosion occurs, when the runaway reconnection begins, either ejective or confined eruption. In ejective eruption, the explosion ejects the erupting flux rope out of the initially closed bipole with opening of the envelope field, while in confined eruption the explosion is arrested and confined within the closed bipole.

In the *break-out model*, proposed by Antiochos et al. (1999), the magnetic reconnection can occur in a curved, horizontal current sheet situated above the magnetic arcade being sheared. This model suggests a multi-flux system which has three neutral lines on the photosphere and four distinct flux systems as shown in Figure 2.3: a central arcade straddling the equator (blue field lines), two arcades associated with the neutral lines (green field lines), and a polar flux system overlying the three arcades (red lines). This model shows two separatrix surfaces that define the boundaries between the various flux systems, and a null point on the equatorial plane at the intersection of the separatrices. This model assumes that the unsheared blue and red fluxes act to confine the expansion of the sheared core field. The CME can occur if the reconnection process at the null point weakens this confinement sufficiently so that the sheared field starts to expand outward rapidly, which drives reconnection ever faster at the null and breaking out to infinity.

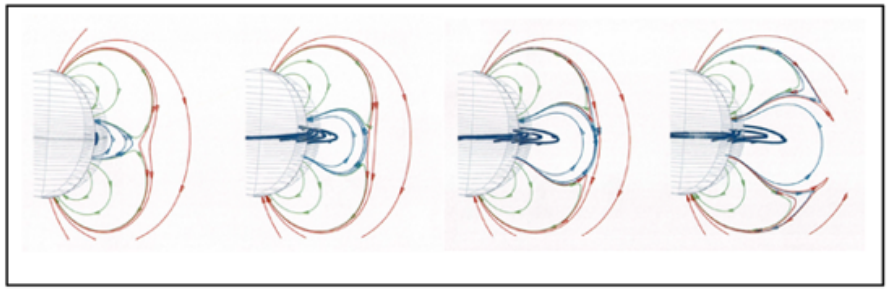

Figure 2.3: The configuration of the breakout-model. The figure is updated by Klimchuk (2001) from Antiochos et al. (1999). The light blue grid indicates to the photospheric boundary surface. The red, green, and blue lines indicate magnetic field lines according to their flux system. Two types of blue field lines are shown, higher lying light blue unsheared field and low-lying dark blue field that is sheared later.

## 2.2 Solar Phenomena and Processes Related to CMEs

Many observations emphasize that CMEs often occur simultaneously with solar flares, prominences, and streamers (e.g. Rust et al., 1980; Gosling et al., 1974; Sheeley et al., 1975; Howard et al., 1985), and most energetic CMEs, propagating in the corona and IP medium, are associated with electromagnetic emissions, shocks, and solar energetic particles (e.g. Sheeley et al., 1983, 1984, 1985; Kahler et al., 1985). These studies have shown that the characteristics of these solar phenomena can significantly contribute to the strength of the CMEs.

### 2.2.1 Prominences

Prominences are great areas of luminous material extending outwards from the solar atmosphere and were first observed during eclipses. They can be observed in the light of $H_\alpha$. Over the photosphere they appear as dark filaments, at the limb as bright structures. Some prominences are short-lived eruptive events (variations within minutes to hours), others can be quiescent and survive many rotational periods of the Sun. The upper parts are often located in the hot corona. Quiescent prominences appear as huge arches of dense cool material embedded in the hot corona. A quiescent prominence may change into an eruptive prominence. At the end of its life, a prominence disperses and breaks up quietly or it becomes eruptive or the matter falls back down the field lines to the photosphere. CMEs are often associated with eruptive prominences. Many studies have emphasized that the eruptive prominence-associated CMEs tend to be less energetic than the large flare-associated CMEs (e.g. Hildner et al., 1977; MacQueen & Fisher, 1983; Gosling et al., 1976).

Some classifications of prominences were proposed in the past, and several studies have been carried out on associating and relating the CMEs with prominences (or filaments). In a study using the Skylab CME observations, 70 % of the CMEs that could be

associated with near-surface activity were associated with eruptive prominences or disappearing filaments (Munro et al., 1979). Based on SMM data, the association between the CMEs and eruptive prominences was 68 % as reported by Webb & Hundhausen (1987) and 76 % as reported by St Cyr & Webb (1991). Gopalswamy et al. (2003) defined prominences as radial and transverse events. They found a strong correlation and a high association rate (83 %) between CMEs and radial prominences, while the association rate was low (24 %) with transverse prominences. Filaments (prominences) are located either above active regions or on quiet Sun. In a study of the relations between filament eruptions, solar flares, and CMEs, Jing et al. (2004) found that 56 % of filament eruption were associated with CMEs. They also found that the active region filaments have a higher flare association rate of 93 % and a lower CME association rate of 43 % compared to quiescent filaments with 27 % and 54 %, respectively. Recent studies indicate that the solar filament eruptions play a crucial role in triggering CMEs (e.g. Schmieder et al., 2013, and references therein).

### 2.2.2 Coronal Streamers

Coronal streamers are quasi-stationary large-scale bright structures in the corona. They are the product of the dynamic equilibrium between confining magnetic fields and expanding hot plasmas, visible in white light or ultraviolet (UV) and extending from the solar surface to IP space (Pneuman & Kopp, 1971; Koutchmy & Livshits, 1992). According to previous studies (e.g. McAllister & Hundhausen, 1996; Subramanian et al., 1999) streamers are closely related to CMEs that present the largest and strongest energy releases in the solar system. In a study of the relations of CMEs and streamers Subramanian et al. (1999) found four types of CMEs with respect to their effects on the streamers. Only ∼16 % of the CMEs disrupted the whole streamer structure. They were called blowout CMEs (Howard et al., 1985; Hundhausen, 1993). About 46 % of the CMEs were overlapping the streamers, but had no effect on them. In ∼9 % of the cases the CMEs created streamer-like structures after they had erupted. About 27 % of the CMEs were latitudinally displaced from the streamers. CMEs in the last two groups were not related to pre-existing streamer structures. Recently, many studies (e.g. Chen et al., 2010, 2011; Feng et al., 2011) have shown that CMEs can interact with streamers, and several studies (e.g. Reiner et al., 2003; Cho et al., 2011; Shen et al., 2013; Chen et al., 2014) have suggested that some radio type II bursts can result from the interactions of CME shocks and streamers in the corona.

### 2.2.3 Shocks

CMEs can cause shocks, when they have speeds faster than the speed of sound in the surrounding solar wind. There are two regions where shocks related to solar eruptions can form: the solar corona and the interplanetary space. These shocks can be sources of secondary effects, such as energetic particles and radio bursts. It has been reported that coronal shocks are short-lived blast-wave shocks induced by flares and confined to the solar corona. Cliver et al. (1999) found that only 5 % of the 2500 hard X-ray flares were associated with coronal shocks, and only 24 % of the 360 largest flares had coronal

shocks, while 65 % of the observed coronal shocks were associated with CMEs. Based on the findings of Cliver et al. (1999), Reames (1999) concluded that a coronal shock is just an early phase of a CME-driven IP shock in most cases.

IP shocks were first directly observed by the Mariner spacecraft in 1962. Hundhausen et al. (1970) used the solar wind observations of the shock disturbances to estimate that a large shock was associated with massive ejections from the Sun. The first direct association between IP shocks and CMEs was suggested by Gosling et al. (1974, 1975, 1976). The early study of Sheeley et al. (1985) showed that 72 % of the shocks were associated with large, low-latitude CMEs on the nearby limb. The speeds of most of the CMEs driving shocks exceeded 500 km $s^{-1}$.

IP shocks in the solar wind can be classified into fast shocks, where the magnetic field increases at the time of the shock passage, and slow shocks, where the magnetic field decreases. In both fast and slow cases, IP shocks are also divided with respect to the solar wind frame of reference to forward shocks that propagate away from the Sun, and reverse shocks that propagate towards the Sun. Fast forward shocks have an increase in the plasma parameters (magnetic field magnitude, solar wind density and temperature), while fast reverse shocks have a decrease in these parameters. In cases of slow forward and reverse shocks, both the solar wind density and temperature are similar for those of the fast forward and reverse shocks, respectively, but the magnetic field magnitude decreases in slow forward shocks and increases in slow reverse shocks. In all cases, the solar wind speed increases (e.g. Richter et al., 1985).

Fast shocks are considered as the most significant manifestations of solar activity in the IP space. They arise from steepening of fast magnetosonic waves. The sources of fast shocks are either fast CMEs or slow-fast stream interaction regions (e.g. Marsden et al., 1987; Lindsay et al., 1994). Most of the fast forward shocks observed at 1 AU are driven by CMEs, and form ahead of IP CMEs, if in the rest frame of the solar wind the IP CME speed exceeds the local magnetosonic speed (see Figure 2.4). Fast reverse shocks are mainly associated with expanding CMEs (e.g. Whang, 1988). Jian et al. (2008) found that most of the CMEs observed at 1 AU (∼66 %) have leading shocks. Slow shocks are only rarely observed in the solar wind (Burlaga & Chao, 1971).

## 2.3 Solar Flares

Solar flares are sudden and intense explosions involving the catastrophic release of magnetic energy in the low corona through magnetic reconnection. They appear as a rapid variation in the brightness on the Sun's surface. Flares were first observed in 1859 by Carrington (1859). The released energy during flares is typically on the order of $10^{20}$ J and up to $10^{25}$ J in powerful flares over short time scales of several tens of seconds to several tens of minutes (e.g. Priest, 1982; Bougeret, 1985). Solar flares are always located near sunspots in the active regions and their frequency follows the 11-year magnetic activity cycle. Solar flares occur when the magnetic field energy built up and stored in active regions in the low corona is suddenly released. During the sudden outbursts of flares, electrons and ions can be accelerated to nearly the speed of light as suprathermal particles. Suprathermal electrons and ions, which remain trapped at the Sun, represent

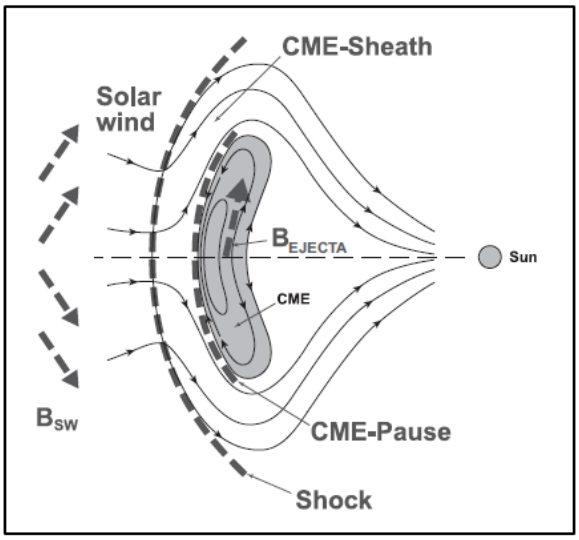


Figure 2.4: The schematic diagram showing a fast CME-driven shock wave in IP space (Evans et al., 2011)

a part of the energy released in flares and produce a wide variety of radiations (Ramaty & Murphy, 1987). The radiation from trapped particles consists in general of three types: continuum emission, which ranges from radio and microwave wavelengths to soft ($\sim$1 – 20 keV) X-rays, hard ($\sim$20 – 300 keV) X-rays, and finally gamma rays (above $\sim$300 keV), which may have energies in excess of 1 GeV; narrow gamma-ray nuclear de-excitation lines between $\sim$4 and 8 MeV; and high-energy neutrons observed in space or by ground-based neutron monitors (e.g. Miller, 1998). In addition to trapped particles, a part can also escape into interplanetary space (e.g. Reames, 1990).

There are different classification schemes of solar flares. The first classification, which has been used since the 1930s, divides the flares into five classes based on the observation of $H_\alpha$ spectral line. These classes are S, 1, 2, 3, and 4 according to the area of the flaring region on the solar disk. S refers to sub-flares (see Table 2.1). The second classification, which was created in the 1970s, divides the flares into five classes based on the soft X-ray peak flux in the 1 – 8 Å band observed by Earth orbiting satellites. The soft X-ray peak flux classes are A, B, C, M, and X, where the letters refer to the order of magnitude of the peak flux (see Table 2.1). Solar flares can also be divided into two classes (Pallavicini et al., 1977): gradual and impulsive according to the temporal profile of the soft X-ray emission. Gradual flares are large, occur high in the corona, have long-duration soft and hard X-rays and gamma rays, are electron poor, are associated with metric-kilometric radio emissions and coronal mass ejections (Sheeley et al., 1975; Kahler, 1977), and produce energetic ions with coronal abundance ratios. Impulsive flares are more compact, occur lower in the corona, produce short-duration radiation, are electron rich, and exhibit dramatic abundance enhancements in certain ions (Reames

Table 2.1: Classification schemes of solar flares

| $H_\alpha$ classification | | Soft X-ray classification | |
|---|---|---|---|
| Class | Area<br>millionths of hemisphere | Class | Peak flux<br>$W\,m^{-2}$ |
| S | $< 100$ | A | $< 10^{-7}$ |
| 1 | $[100-250)$ | B | $[10^{-7}-10^{-6})$ |
| 2 | $[250-600)$ | C | $[10^{-6}-10^{-5})$ |
| 3 | $[600-1200)$ | M | $[10^{-5}-10^{-4})$ |
| 4 | $> 1200$ | X | $> 10^{-4}$ |

et al., 1994).

Interrelations of CMEs and flares are not yet fully clear due to the lack of high-quality CME observations in the low corona, where CMEs are initiated and accelerated (e.g. Klimchuk, 2001). Several observational facts regarding the relationship between CMEs and flares based on statistical studies have been presented during the previous four decades. The flare occurrence rate is much larger than that of CMEs because not all flares are associated with CMEs (Lee et al., 2016, and references therein). The probability of association between CMEs and flares tend to increase monotonically with the duration of the flare (e.g. Sheeley et al., 1983; Harrison, 1995) and the size of the soft X-ray flare (e.g. Yashiro et al., 2006). Kahler et al. (1989) revealed a good relationship between the flare duration and the CME angular width, and found that the locations of flares on the solar disk could be anywhere within the CME angular span. Many studies have shown that a synchronization process exists between the CME and flare development phases (e.g. Zhang et al., 2001, 2004; Zhang & Dere, 2006; Gallagher et al., 2003; Vršnak et al., 2004). Zhang et al. (2001) have shown that the CME initiation phase always occurs before the onset of the associated flare. Then, the CME displays an impulsive acceleration phase that coincides very well with the flare's rise phase lasting for a few to tens of minutes. The acceleration of CMEs ceases near the peak time of the soft X-ray flares.

# Chapter 3

# Solar Electromagnetic Emissions

Electromagnetic (EM) emission is a phenomenon by which energy escapes from the Sun at the speed of light in the form of waves. Several types of EM emissions, that can be expressed in terms of energy, wavelength or frequency, emit from the Sun due to either characterizing the plasma temperature in the solar atmospheric layers or due to mechanisms occurring during solar eruptions. The Sun emits gamma rays, X-rays, ultraviolet, visible light, infrared, and radio waves. The photosphere, where the temperature is $\sim$6000 K, is a source of the white light, while the ultraviolet emits from the chromosphere where the temperature is $\sim 10^4$ K. The corona with a temperature of about $\sim 10^6$ K is a source of extreme ultraviolet (EUV) radiation and X-rays, while gamma rays are emitted in processes associated with solar flares.

The sudden enhancement of electromagnetic emissions in $H_\alpha$, ultraviolet, X-rays, and radio wavelengths are frequently associated with powerful CME-associated flares (e.g. Joshi et al., 2007). Radio emission from an undisturbed plasma is generated by bremsstrahlung (free-free emission) resulting from the Coulomb interaction of the plasma electrons with ions, and by gyroresonance emission of electrons in the presence of a magnetic field. Radio emission produced by nonthermal electrons is attributed principally to gyrosynchrotron and coherent plasma emission. Gyrosynchrotron emission usually dominates at frequencies above $\sim$3 GHz. Coherent plasma emission, which most often dominates at frequencies below 3 GHz, is caused by plasma instabilities driving various wave modes that produce observable radio waves (e.g. Pick, 2004).

## 3.1 X-Rays

Since the Sun's coronal plasma is hot, it emits low-energy X-rays. During solar flares the plasma is heated to a temperature of about $\sim$10 MK and electrons accelerated to very high energies cause a sudden enhancement of radiative flux at X-ray wavelengths rising above the background. X-ray wavelengths lie between UV and $\gamma$-rays in the electromagnetic spectrum, in the range of $\sim$0.01 nm to $\sim$10 nm corresponding to energies in the range of $\sim$100 eV to $\sim$100 keV. Because the Earth's atmosphere totally absorbs X-rays coming from the Sun, X-rays must be observed by spacecraft above the atmosphere.

X-ray flares can be divided into two sub-types according to their energies: hard X-rays and soft X-rays.

*Hard X-rays* have relatively high energies in the range $\sim$10 – 100 keV. They are emitted during the early impulsive phase of solar flares where electrons accelerated to very high energies emit non-thermal bremsstrahlung (e.g. Lin & Hudson, 1976). Hard X-rays can be used as an important information source for understanding the energy release process and the mechanism of particle acceleration during flares (Dennis, 1988).

*Soft X-rays* have lower energies in the range $\sim$1 – 10 keV. They gradually build up and peak a few minutes after the impulsive emission of hard X-rays and start to gradually decrease during the gradual phase of a solar flare. Soft X-rays are thermal radiation produced by the bremsstrahlung processes. Soft X-ray flux can be used for characterizing the strength of a solar flare. The strongest flares have high soft X-ray peak fluxes and weak flares have lower peak fluxes (see Table 2.1) (see also Isola et al., 2007).

Many studies have investigated the correlations between the characteristics of CMEs and the associated soft X-ray peak fluxes. The correlation coefficient between the soft X-ray flare intensities and the associated CME speeds has been found to be $\sim$0.53 (e.g. Hundhausen, 1999; Moon et al., 2002)). Applying certain temporal and spatial constraints, the correlation coefficient has been reported to increase up to 0.76 (Mahrous et al., 2009) or 0.65 (Youssef, 2012). Salas-Matamoros & Klein (2015) found that a correlation between the CME speed and the soft X-ray flux and fluence of the associated flares were 0.48 and 0.58, respectively. The correlation can be even higher, if the CMEs are associated with long-duration flares (Bąk-Stęślicka et al., 2013), or if the CME-associated flares are also related to type II bursts (Shanmugaraju et al., 2011).

## 3.2 $H_\alpha$ Emission

$H_\alpha$ has a wavelength of 656.281 nm, and is visible in the red part of the electromagnetic spectrum. It occurs when the electron of a hydrogen atom falls from its third to second lowest energy level. This process occurs in the Sun's chromosphere where the temperature is about $\sim 10^4$ K. The sudden enhancement of radiative flux of $H_\alpha$ can occur during solar flares. Early statistical studies showed that most flares with $H_\alpha$ emission were associated with CMEs with an association rate of $\sim$90 %, while 40 % of CMEs were associated with $H_\alpha$ flares (Munro et al., 1979). In a subsequent study, Antalova (1985) showed that the duration of $H_\alpha$ flares reflects the quantitative variation of the gradual phase of the flares. They found that the mean duration of $H_\alpha$ flares associated with type II radio bursts is shorter than that of the flares which are accompanied by type IV bursts. $H_\alpha$ observations are used to describe the shape, size, location, and intensity of solar flares in the chromosphere. This has lead to a flare classification scheme based on the extent and brightness in $H_\alpha$ emission (see Table 2.1).

## 3.3 Ultraviolet Radiation

In general the ultraviolet radiation is produced by heating the body to a sufficient temperature. Solar ultraviolet radiation is emitted from the hot corona of the Sun and was

first detected by instruments built by Richard Tousey and colleagues at the US Naval Research Laboratory in the late 1940s. It contributes about 10 % of the total radiative output of the Sun. It has wavelengths from 10 nm to 400 nm, shorter than that of visible light but longer than X-rays. Based on the wavelength range, UV radiation can be divided in four common sub-types: near UV (300 – 400 nm), middle UV (200 – 300 nm), far UV (122 – 200 nm), and extreme UV (10 – 121 nm). The extreme UV is most commonly used to observe solar phenomena; for example the Extreme ultraviolet Imaging Telescope on the SOHO spacecraft observes Fe XII at 19.5 nm. By UV and EUV emissions, the plasma properties (e.g., densities, temperatures, outflow velocities, and elemental abundances) in the corona can be determined from remote sensing diagnostics (Moses et al., 2015).

## 3.4 Radio Emissions

The Sun's atmosphere emits radio waves in a frequency range covering over seven orders of magnitude from a few tens of kHz up to a few tens or hundreds of GHz. Solar radio emission arises from several different processes and can be divided into three main components: The quiet component is thermal emission from the hot ionized plasma and occurs around the time of the sunspot minimum. The slowly varying component is also thermal emission in origin but it arises from regions in the chromosphere and corona around and above active regions where the electron density is higher. Thus the radio flux density is highly correlated with the sunspot number and follows the 11-year sunspot cycle. The burst component is non-thermal emission and occurs during explosive energy release in the Sun's atmosphere. The radio emission of the burst component has an energetic and explosive characteristic, which can increase up to a million times the normal intensity in just a few seconds.

The solar radio bursts are considered as significant manifestations of powerful solar events. They provide an important diagnostic tool for specifying the magnetic and temperature structure at the time of the event. They also provide evidence for electrons accelerated to very high speeds as well as powerful shock waves. Radio bursts are not observed simultaneously at all frequencies, but frequencies usually drift down and lower frequencies are observed later in time. This is explained by a disturbance that travels out through the progressively more rarefied layers of the solar atmosphere, making the local electrons in the corona vibrate at their natural frequency of oscillation called the plasma frequency.

The first detection of solar radio emission was by Hey et al. (1946) who reported that metric solar emission had been observed by the British army equipment on February 27 and 28, 1942. The first radio classifications scheme was developed by Australian and French solar radio astronomers during 1950s.

The dynamic spectra of solar radio bursts between 10 MHz and 8000 MHz are observed by ground-based instruments. Because the radio spectrum with frequencies below 10 MHz is reflected by the Earth's ionosphere and can not reach the ground, this part of the radio spectrum is observed by spacecraft lofted above the Earth's ionosphere. Based on the dynamic spectrum, the solar radio bursts can be classified into radio type

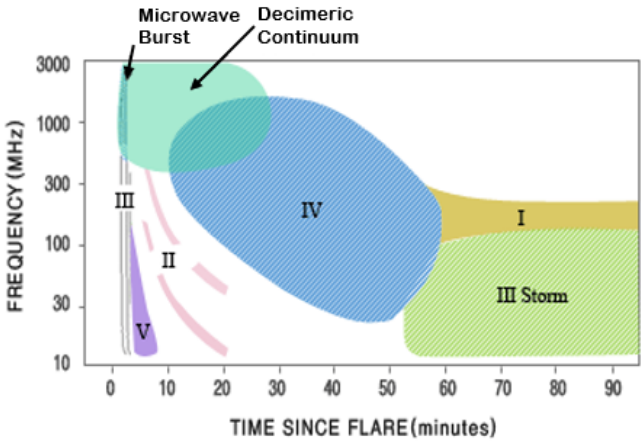


Figure 3.1: Schematic diagram of the solar radio emission types showing the radio bursts classification as function of frequency and time. The image was taken from http://sunbase.nict.go.jp/solar/denpa/hiras/types.html.

I, type II, type III, type IV, and type V bursts (see Figure 3.1).

### 3.4.1 Type I

Radio type I burst is composed of short duration radio enhancements at metric wavelengths, superimposed on a broad frequency band continuum (McLean & Labrum, 1985). It is also called a noise storm and was first reviewed by Elgaroy (1977). The noise storms are the most common type of activity observed on the Sun's corona at meter wavelengths. They are associated with active regions, but not related to a flare, and they can last from hours to days (Le Squeren, 1963). Noise storms are attributed to electrons accelerated to modest energies of a few keV within large-scale magnetic loops that connect active regions to more distant areas of the Sun (e.g. Mercier et al., 1984).

### 3.4.2 Type II

Type II radio bursts are produced by non-thermal electrons accelerated in magneto-hydrodynamic shocks propagating from low corona into interplanetary space with the emission frequency slowly drifting from high to lower frequencies due to decreasing electron density encountered by the shock in the corona (e.g. Cairns et al., 2003). The shocks occur in different parts of the solar atmosphere. Metric type II bursts are generated by coronal shocks, and type II bursts from decametric-hectometric to kilometric wavelength range are generated by IP shocks (Wagner & MacQueen, 1983). Metric type II bursts are associated with flares, and may be produced by blast waves in the low corona, and most often vanish before reaching the high corona, while IP type II bursts are excited by CME-driven shocks formed, most often, in the high corona (e.g. Cane & Erickson, 2005). Metric and IP type II bursts, when observed together, have distinct drift rates. It cannot be excluded, that metric and IP type II bursts are produced by the

same shock, but from different sections of the shock front, the metric component coming from the flanks and the IP component from the nose of the shock (Raymond et al., 2000).

The first identification of coronal type II bursts was by Payne-Scott et al. (1947), who showed that the meter wavelengths from the disturbed Sun are characterized by the occurrence of sudden large increases in intensity of a duration of several seconds or minutes. Wild & McCready (1950) classified the type II bursts as slow-drifting bands in the dynamic spectra to distinguish them from the fast-drifting bands of type III bursts. IP type II bursts were first discovered in spacecraft data by Malitson et al. (1973). Many IP type II bursts were subsequently identified from different spacecraft (e.g. Boischot et al., 1980; Cane et al., 1982).

In type II bursts, the radio emission may demonstrate two characteristic bands differing in the frequency by a factor of approximately 2. They are interpreted in terms of a shock wave accelerating electrons, which in turn are driving Langmuir waves near the electron plasma frequency, and producing radio emission near the local plasma frequency (fundamental) and its second harmonic (Wild & McCready, 1950; Wild et al., 1954; McLean & Labrum, 1985). In addition, each of these bands can further split into two (or more) thinner lanes approximately parallel to each other (McLean & Labrum, 1985). This phenomenon is known as band-splitting. Many theories have been proposed to explain the underlying processes in the band-splitting, but they are still under debate.

Type II bursts can be classified into many sub-types according to the range of their frequencies (or wavelengths) in the dynamic spectrum. Type II bursts that start and end within the metric (m) wavelength domain ($> 20$ MHz), in the decameter-hectometric (DH) wavelength domain ($1 - 14$ MHz), or in the kilometric (km) wavelength domain ($< 1$ MHz) are referred to as purely m type II, purely DH type II, or purely km type II bursts, respectively. Some bursts have counterparts in all the wavelength domains and are referred to as m-km type II bursts, while in many events type II bursts have m-DH or DH-km components as a separate feature (e.g. Gopalswamy, 2010b, and references therein) (see Figure 3.2a).

The characteristics of CMEs depend on the wavelength range of associated type II bursts. The average speed, angular width, halo fraction, and deceleration in the field of view of white-light coronagraphs of CMEs progressively increase from purely m (610 km s$^{-1}$, 96°, 3.8 % and $-3$ m s$^{-2}$) to DH (1115 km s$^{-1}$, 139°, 45 % and $-7$ m s$^{-2}$) to m-km (1490 km s$^{-1}$, 171°, 71.4 % and $-11$ m s$^{-2}$) type II bursts, respectively (Gopalswamy et al., 2005). The purely km type II bursts have CME characteristics approximately similar to those of the purely m type II bursts, but they are accelerating (539 km s$^{-1}$, 80°, 17.2 % and 3 m s$^{-2}$, respectively) (Gopalswamy, 2006b).

CMEs associated with type II radio bursts are known as radio-loud (RL), while those without radio type II burst association are known as radio-quiet (RQ). In a study of the characteristics of CME-driven shocks with respect to solar type II radio bursts, Gopalswamy et al. (2010) found that a large fraction (66 %) of CME-driven shocks were RL, while 34 % were RQ. The CMEs associated with RL shocks have faster speeds, wider angular widths, they have negative acceleration, and are associated with higher peak fluxes of soft X-rays compared to those of the RQ shocks. The CME source

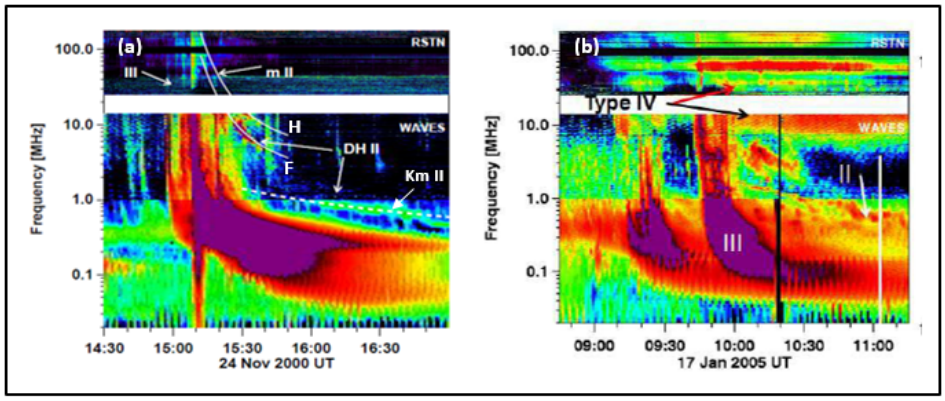


Figure 3.2: (a) Composite dynamic spectrum from the ground based Radio Solar Telescope Network and Wind/WAVES observations showing Type II and III bursts on 2000 Nov 24. (b) Type IV burst on 2005 January 17 extending from above 180 MHz down to ∼3 MHz. The symbols mII, DHII, KmII, refer to metric, decameter-hectometric, and kilometric type II bursts, while F and H refer to fundamental and harmonic lanes of m-DH type II bursts.

locations of RQ shocks are concentrated near the central meridian, while those of RL shocks are more widely distributed. The average speed, transit speed, and Alfvénic Mach number for the RL shocks are larger than those of the RQ shock. This indicates that the CME-driven shocks associated with RL events are more energetic than those associated with RQ events.

### 3.4.3 Type III

Type III bursts are thought to be produced by electron beams propagating along open magnetic field lines through the coronal and IP plasma via the plasma emission mechanism (e.g. Ginzbursg & Zheleznakov, 1958; Wild & Smerd, 1972). Type III bursts were first discovered at metric wavelengths in the frequency range 10 to 500 MHz by ground-based telescopes (Wild & McCready, 1950), while in the IP space they were first detected by the radio instruments on Alouette-I and by later space radio experiments such as ISEE-3, Ulysses, Geotail, and Wind (e.g. Hartz, 1964, 1969; Fainberg & Stone, 1970; Bougeret et al., 1998).

In the dynamic spectrum, the type III bursts are characterized with the high drift rate from high to low frequencies and thus appear as almost vertical features (see Figure 3.2a). In the inner corona, type III bursts can be observed as a couple of variant types such as the J and U bursts, due to electron beams propagating along closed field lines. They are often observed with reverse drift due to electrons propagating towards the Sun. The reverse-drift bursts are closely associated with hard X-rays. In IP medium, there are three low-frequency variants of type III bursts that originate from three different sources: isolated type III bursts, complex type III bursts, and type III storms (Gopal-

swamy, 2004a; Nindos et al., 2008).

*Isolated type III bursts* are the most common class of type III bursts in the IP medium. They are produced by energetic electrons escaping from flares and small-scale energy release sites in the low corona. *Complex type III bursts* are produced by electron beams accelerated in blast-wave shocks and injected along open magnetic field lines (Cane et al., 1981). They occur in conjunction with CMEs. Complex type III bursts were first identified at hectometric wavelengths in the ISEE-3 data by Cane et al. (1981) and Cane & Stone (1984) who named them "shock accelerated" events. Gopalswamy et al. (2000) found that most of the CME-driven shocks ($\sim 92\,\%$) had a long-duration type III burst. *Type III storms* are produced by low-energy electrons ($\sim 2\,\mathrm{keV}$) from small-scale, quasi-continuous energy releases into closed magnetic structures of active regions. They are weak dekametric-to-kilometric radio burst activity and consist of thousands of short-lived type III bursts in rapid succession and can last for days to weeks (e.g. Fainberg & Stone, 1970; Potter et al., 1980). Type III storms are known to be associated with metric type I bursts, which in turn are associated with solar active regions.

### 3.4.4 Type IV

Type IV bursts are quasi-continuum radio emissions with a duration of a few minutes to a few hours that occur in conjunction with flares and coronal mass ejections. They are caused by energetic electrons trapped within magnetic structures and plasma (Benz, 1980). Metric type IV bursts are non-thermal in nature and can be classified into two categories, stationary and moving. The former show no systematic movement and their sources may be energetic particles trapped in post-flare loops and arcades. The latter show frequency drifts towards the lower frequencies, and their sources are mostly energetic particles trapped in rising CME structures (e.g Nindos et al., 2008).

Rarely the moving type IV bursts may extend in dynamic spectra to the hectometric wavelengths (e.g. Gopalswamy, 2004b; Hillaris et al., 2016) (see Figure 3.2b). Hillaris et al. (2016) have suggested that moving type IV bursts are caused by second harmonic plasma emission from the enhanced electron density in the CME leading edge. From the observed spectrum characteristics, moving type IV bursts can be interpreted as Razin suppressed gyrosynchrotron emission from nonthermal electrons trapped in moving magnetic structures (e.g. Bastian et al., 2001).

Moving type IV bursts appear to be highly related to CMEs because the radio emitting structures move as expanding arches or advancing fronts associated with CMEs (Gopalswamy, 2004b). They are observed in association of very fast ($\sim$1526 $\mathrm{km\,s^{-1}}$) and very wide (316°) CMEs indicating that they are caused by very high-energetic CMEs. According to the Wind/WAVES observations, the minimum frequency of these bursts ranges from $\sim 2\,\mathrm{MHz}$ to $\sim 14\,\mathrm{MHz}$ with an average of 6.6 MHz (Gopalswamy, 2004c, 2010b).

### 3.4.5 Type V

Type V bursts are broad-band continuum radiation, appearing at meter wavelengths for a few seconds or a minute as diffuse continua in dynamic spectra. They were first classified as a special spectral class by Wild et al. (1959a). Two early studies proposed physical processes responsible for the type V bursts. Wild et al. (1959b) proposed that the synchrotron radiation from relativistic electrons is responsible for these bursts, while Weiss & Stewart (1965) rejected the synchrotron radiation and proposed forward plasma radiation as the emission process of type V bursts. A recent study of Tang et al. (2013) proposed that type V bursts are excited by the coherent radiation (electron cyclotron maser) instability.

Type V bursts are usually following type III bursts or type III burst groups (Wild et al., 1959a). Type V and III bursts are closely associated and may be produced by the same physical process (Wu et al., 2002). Type V and III bursts originate from almost the same average height, but type V sources are usually displaced from type III sources by a few tenths of a solar radius or more. Type V bursts originate from larger sources compared to those of type III bursts, and the size of these sources increases greatly as the frequency decreases. The high frequency limit of type V bursts is in the range of 120 – 200 MHz, and type V radiation has not been observed at a frequency lower than 1 MHz. The duration of type V bursts increase with decreasing frequency, with an average range from ∼40 s at 200 MHz to ∼200 s at 20 MHz (Tang et al., 2013).

# Chapter 4

# Solar Energetic Particles

Solar Energetic Particle (SEP) events, consisting of protons, electrons, and heavier nuclei such as He-Fe, are accelerated at the Sun or in the IP medium during solar eruptions, and propagate along IP magnetic field lines from the Sun to the Earth. They have been observed near the Earth with energies ranging from some keV nucleon$^{-1}$ to more than 1 GeV nucleon$^{-1}$, and occur in events that last from some hours to a few days with intensity enhancements above the quiet-time background by many orders of magnitude. The first SEP event with energies up to GeV was observed by ground-based ionization chambers in the mid 1940s by Forbush (1946). SEP events are one of the most interesting phenomena in solar physics. The characteristics of SEP events such as the time-intensity profiles, energy spectra, ionization states, and abundances of elements and isotopes can carry information of the properties of their source plasma and the physical mechanisms of their acceleration (e.g. Reames, 1999).

## 4.1 Sources of Solar Energetic Particles

For past decades, it was thought that solar flares were the main sources of the major IP particle events. In early studies, Forbush (1946) and Meyer et al. (1956) detected that cosmic ray intensity enhancements were associated with large solar flares and they suggested that such large flares might be capable to accelerate the charged particles up to GeV energies. However, the evidence obtained in subsequent several studies during the 1990s (e.g. Reames, 1990, 1995, 1999; Kahler, 1992; Gosling, 1993; Cane, 1995) suggested that the shock waves driven out from the corona by CMEs are responsible for the energetic particle acceleration observed in large events.

Currently, there is no doubt that both solar flares and CME-driven shocks are the main sources of SEPs observed at Earth, but the controversial issue regarding SEP production is whether the bulk of the acceleration occurs in the low corona in coronal shocks formed by solar flares, or whether it occurs in travelling IP shocks associated with CMEs. Some studies (e.g. Gosling, 1993; Reames et al., 1996) suggest that if the bulk of SEP acceleration is due to coronal shocks in the low corona, then solar flares are the major accelerator. But if the bulk of acceleration occurs in IP medium, then CME-driven shocks are the major accelerator and hence flares will be a minor source or even do not contribute in SEP acceleration. Kahler (1994) has suggested that the

prompt component of SEP events could be attributed to acceleration by coronal shocks in the low corona at early times in the eruption, whereas the delayed component is accelerated by the CME bow shocks in the high corona or IP medium. Many studies (e.g. Reames, 1990) have suggested that the CME-driven shocks are the main accelerator for the high-energy SEP events with energies up to 10 MeV.

## 4.2 SEP Classification

A two-class paradigm of SEP events, impulsive and gradual (see Figure 4.1), was largely accepted in the 1990s (e.g. Reames, 1999, 2013; Cliver, 2000). The impulsive events are thought to be related to solar flares. They occur in the low corona, last for a few hours and are typically observed when the observer is magnetically well connected to the flare site. They are electron-rich and associated with type III radio bursts. They also have $^3$He/$^4$He ratios enhanced by factors $10^3 - 10^4$, and enhanced Fe/O ratios by a factor of 10 over the nominal coronal values, and Fe ionization states of up to 20. In gradual events particles can be accelerated up to much higher energies in CME-driven shocks. They occur in the high corona or in IP medium and last for several days and are observed from wide range of solar longitudes. They are proton-rich, and associated with type II radio bursts, and have average Fe/O ratios of 0.1 and Fe ionization states of 14.

Based on more recent observations some studies (e.g. Kocharov & Torsti, 2002; Kallenrode, 2003) have suggested that there are also hybrid/mixed event cases. The hybrid/mixed events have characteristics of both impulsive and gradual events. Such events represent a challenge to the two-class paradigm of SEP events. In a recent study, Papaioannou et al. (2016) presented a statistical study of the characteristics of 314 SEP events extending over a large time span from 1984 to 2013. They found that most of the SEP events in their catalogue do not conform to a simple two-class paradigm.

## 4.3 SEP Acceleration Mechanisms

The observations of the characteristics of impulsive and gradual SEP events led to the general scenario that energetic particles are accelerated by different mechanisms, but there is ongoing debate about the relative roles of these mechanisms.

### 4.3.1 Acceleration in Solar Flares

The characteristics of the elemental and isotopic composition in impulsive events requires a mechanism that is highly variable with rigidity. Based on $^3$He-rich flares, Kocharov L. G. & Kocharov G. E. (1984) suggested the process of selective heating (see also Reames, 1990). In this scenario, particles are accelerated by a process related to magnetic reconnection in a compact closed magnetic field loop and are confined in the magnetic field structure (see Figure 4.2a). When the confined particles interact with the denser solar atmosphere, hard electromagnetic radiation is created. The electromagnetic waves are excited by electron beams moving back and forth along the loop. These

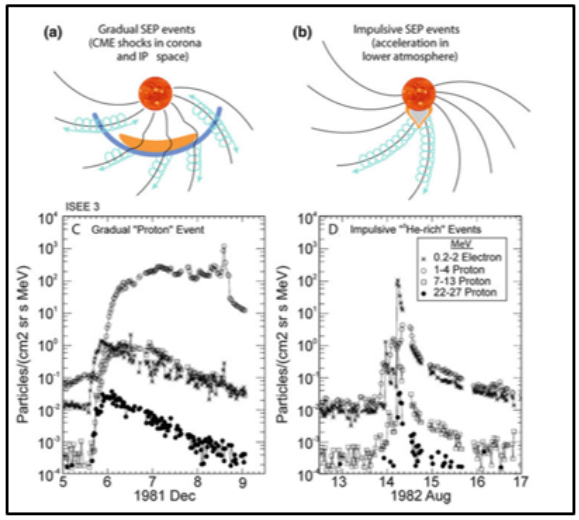


Figure 4.1: The two-class paradigm of SEP events showing the gradual (a) and impulsive (b) SEP events. Comparison of intensity-time profiles of electrons and protons in pure gradual (c) and impulsive (d) SEP events (Desai & Giacalone (2016) reproduced from Reames (1999)).

waves propagate across the field and, on absorption by the local plasma, accelerate particles. The acceleration occurs for the particles with gyro-frequencies comparable to the wave frequency, thus different waves accelerate different particles. The major species of particles, such as H and $^4$He, absorb most of the wave energy inside the loop while the minor species, such as $^3$He, are in resonance with the waves. These latter particles are preferentially accelerated on open field lines and escape into interplanetary space (see also, Kallenrode, 2003).

### 4.3.2 Acceleration in CME-driven Shocks

In gradual events, particles are accelerated out of the ambient plasma at CME-driven shocks via three possible processes. In *shock drift acceleration*, the acceleration occurs because the particle's orbit in the electric and magnetic fields at the shock results in an overall drift which converts electric potential energy to kinetic energy (e.g. Decker, 1988). It works best for the quasi-perpendicular shocks and is characterized by a shock spike around the time of shock passage. In *diffusive shock acceleration*, based on first-order Fermi acceleration, the accelerated particles can be mobile enough to cross the shock many times and because of that they absorb the energy from the background medium by scattering off the magnetic irregularities converging at the shock (e.g. Forman & Webb, 1985). This mechanism dominates at quasi-parallel shocks and leads to smoother variations and a long-lasting high intensity in the event. In *stochastic acceleration*, charged particles gain energy when they are moving under the influence of

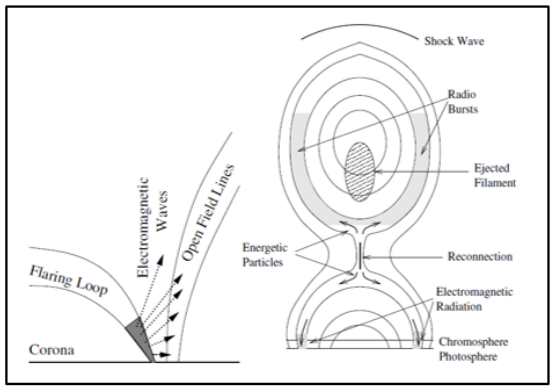


Figure 4.2: The schematic diagram of particle acceleration in impulsive (a) and gradual (b) events (Kallenrode, 2003).

randomly time-varying electromagnetic fields. This is a second-order Fermi acceleration and works in the turbulence behind the shock front (e.g. Sturrock , 1966). It can be seen as a sudden increase in intensity in the turbulent zone behind the shock.

The configuration of particle acceleration in SEP events associated with gradual flares and CMEs is shown in Figure 4.2b. The particle acceleration occurs in two places: Escaping particles are accelerated at the shock in front of the CME. Particles accelerated in the reconnection region below the core of the CME precipitate into the denser solar atmosphere and produce electromagnetic radiation and they are thought to be trapped below the CME (Kallenrode, 2003).

## 4.4 Relations of SEP Characteristics with Solar Events

Several studies have investigated the dependence of SEP characteristics on various CME (e.g. Kahler, 2001; Park et al., 2012), solar flare (e.g. Kurt et al., 2004; Cliver et al., 2012) and both CME and flare characteristics (e.g. Hwang et al., 2010; Dierckxsens et al., 2015). It was found that the correlation coefficients between the logarithms of SEP peak intensities and the flare parameters (soft X-ray peak flux, solar location) as well as the CME parameters (speed and angular width) varied broadly in the range 0.4 – 0.6. Park et al. (2012) found that the occurrence probabilities of SEP events depend on the CME speed, location, and angular width. They also found that the relationship between the CME speed and SEP flux depend on the CME longitude, angular width, and direction parameter. Dierckxsens et al. (2015) (see also Papaioannou et al., 2016) showed that the correlation between the proton peak flux and the CME speed decreases with increasing proton energy, while the correlation with the flare intensity showed the opposite behaviour.

On the other hand, many studies (e.g. Wang, 2005; Gopalswamy et al., 2008, 2005; Cane et al., 2010; Richardson et al., 2014; Papaioannou et al., 2016) have investigated the relationships between the SEP characteristics and solar radio bursts, in addition to

both CME and flare characteristics. Cliver et al. (2004) discovered that 25 % of the radio bursts observed only at metric wavelengths were associated with SEP events at Earth, but the association increased to ∼90 %, when the metric type II bursts were accompanied by DH type II emission. Gopalswamy et al. (2005) showed that the majority (78 %) of the type II bursts at different wavelengths were associated with SEP events. Cliver & Ling (2009) found that gradual SEP events were highly associated (96 %) with DH type II bursts versus only low association rate (5 %) for the impulsive events, while Miteva et al. (2013) showed that both gradual and impulsive SEP events have highest association with type III radio bursts, and lower association with type II.

## 4.5 Energetic Storm Particles

Energetic storm particle (ESP) events refer to the enhancements of energetic particles such as protons, electrons, and ions observed during the passing of an IP shock with the observer (e.g. Cohen, 2006; Mäkelä et al., 2011). Bryant et al. (1962) were the first to discover ESP events. By examining Explorer 12 data they noted large flux increases of 2 – 15 MeV protons occurring just before a storm sudden commencement and two days after a solar flare.

Sarris & Van Allen (1974) proposed a two category system for ESP events based on the observed particle intensities: spike events and classic events. In spike events, the time profiles of the ESP events show a rapid change in particle intensities (short-duration). The maximum energy at which the proton intensity increases is rarely observed to exceed 5 MeV. These events are a result of the shock drift acceleration at quasi-perpendicular shocks. In classic events, the time profiles of the ESP events show a gradual change in particle intensities, increasing slowly before peaking near the time of the shock passage and followed by a slow decrease (long-duration). ESP events can last for several hours and might arrive ahead or behind the shock. The maximum energy at which the proton increases are observed in classical event is higher than in spike events, extending to well above ∼20 MeV. The source of the classic ESP events is diffusive shock acceleration at quasi-parallel shocks.

Several studies have investigated the dependence of ESP events on their solar sources and shock characteristics. Lario et al. (2005) showed that stronger and faster shocks more likely influence local particle fluxes, but they did not find any strong correlations between the shock parameters and the ESP event characteristics. Ho et al. (2008) showed that 64 % and 31 % of the shocks exhibited an ion flux enhancement in the 47 – 68 keV and 1.9 – 4.8 MeV energy range, respectively, and electron flux enhancement in the 38 – 53 keV energy channel were observed in 20 % of the events. In a study of ESP events above 1.5 MeV associated with fast forward shocks, Huttunen-Heikinmaa & Valtonen (2009) found that only 40 % of the observed interplanetary fast forward shocks accelerate ESPs and that the high-energy ESP-effectiveness of the fast forward shocks has a solar cycle dependence. In an investigation of ESP events associated with IP shocks driven by CMEs, Mäkelä et al. (2011) found that the CMEs were significantly more energetic and Alfvénic Mach numbers were significantly higher in the shocks producing ESP events compared to those in the shocks without an ESP event. They also

found that $\sim$52 % of the RL shocks and only $\sim$33 % of the RQ shocks produced an ESP event at proton energies above 1.8 MeV, and that ESP event sizes showed a modest positive correlation with the CME and shock speeds.

# Chapter 5

# Geomagnetic Storms

A geomagnetic storm is defined as a temporary disturbance of the Earth's magnetosphere that occurs when an intense and long-duration interplanetary magnetic field efficiently exchanges energy with the Earth's magnetosphere-ionosphere leading to an intensified magnetospheric ring current (e.g. Gonzalez, 1994). Various indices can be used to measure the level of geomagnetic activity and to assess the severity of magnetic storms. Disturbance storm-time (Dst) index and $K_p$ index are most commonly used to measure the level of geomagnetic activity. The Dst index represents the average change in the horizontal component of the Earth's magnetic field (in units of nT) during one-hour interval at four low latitude stations and depends on the strength of the magnetospheric ring current (Sugiura, 1964). The $K_p$ index quantifies the maximum disturbances in the horizontal component of the Earth's magnetic field during a three-hour interval observed from ground-based magnetometers around the world (Bartels et al., 1939). A geomagnetic storm often consists of three phases: The initial phase is manifested by the increase of the middle-latitude horizontal magnetic field intensity at the surface of the Earth. In the main phase the horizontal magnetic field at middle latitudes strongly decreases. During the recovery phase the depressed horizontal magnetic field component returns to normal levels. Since the initial phase is eventually followed by the main phase, it is called the storm commencement (e.g. Lindsay et al., 1995).

## 5.1 Classification of Geomagnetic Storms

Geomagnetic storms can be classified into five groups based on the minimum value of Dst (Loewe & Prölss, 1997): weak ($-50\,\text{nT} < \text{Dst} \leq -30\,\text{nT}$), moderate ($-100\,\text{nT} < \text{Dst} \leq -50\,\text{nT}$), strong ($-200\,\text{nT} < \text{Dst} \leq -100\,\text{nT}$), severe ($-350\,\text{nT} < \text{Dst} \leq -200\,\text{nT}$), and great ($\text{Dst} \leq -350\,\text{nT}$). Geomagnetic activity with $\text{Dst} > -30\,\text{nT}$ can be described as quiet, while all storms with $\text{Dst} \leq -100\,\text{nT}$ are sometimes classified as intense (Gonzalez, 1994). The National Oceanic and Atmospheric Administration classifies geomagnetic storms based on the $K_p$ index into a five-level system called the G-scale, to indicate the severity of observed geomagnetic activity. The G-levels with their $K_p$ values and storms levels are the following: G1 level (minor; $4 \leq K_p < 5$), G2 level (moderate; $5 \leq K_p < 6$), G3 level (strong; $6 \leq K_p < 7$), G4 level (severe; $8 \leq K_p < 9$), and G5 level (extreme; $K_p = 9$).

## 5.2 Sources of Geomagnetic Storms

The major cause of geomagnetic storms is intense, long-duration southward magnetic field component ($B_s$) in the IP magnetic structure. The strong $B_s$ in the IP magnetic field can be caused by IP disturbances driven by CMEs (Klein & Burlaga, 1982), high-speed streams (HSS) from coronal holes (Sheeley et al., 1976), and corotating interaction regions (CIRs) (Rosenberg & Coleman, 1980) (see also, Gonzalez, 1994; Lindsay et al., 1995; Xu et al., 2009; Zhang & Moldwin, 2014, and references therein). CIR is an interaction region forming between the high and slow solar wind streams when the high-speed stream collides with the preceding slow solar wind (Smith & Wolf, 1976). CIRs can consist of three subregions: the leading half (the increased low-speed flow), the stream interface, and the trailing half (the decreased HSS) (e.g. Richardson et al., 2006).

The IP counterparts of CMEs are known as ICMEs. Some ICMEs drive IP shocks. ICMEs typically consist of three subregions: shock, sheath region immediately after the shock, and the following driving ejecta. The sheath is compressed heliospheric magnetoplasma accumulated as the CME erupts and propagates into the IP medium (e.g. Gopalswamy, 2008). Almost one-half of the ICME-driven ejecta typically contain a so-called magnetic cloud. A magnetic cloud is a magnetic flux rope with a large scale smoothly rotating magnetic field, and is characterized by a low proton temperature, a low proton plasma $\beta$ (ratio of the plasma pressure to the magnetic pressure), and has a field intensity larger than the surrounding IP field (e.g. Klein & Burlaga, 1982). Other ICME-driven ejecta without smooth magnetic flux-rope structures are called non-cloud ICMEs (e.g. Cane et al., 1997). The increase in plasma ram pressure associated with the increase in the density and speed at and behind the shock cause the initial phase of a geomagnetic storm. The $B_s$ in either the sheath or ejecta is responsible for the storm main phase (e.g. Tsurutaini & Gonzalez, 1997).

## 5.3 Generation of Geomagnetic Storms

Geomagnetic storms are produced when energy is transferred from the solar wind into the Earth's magnetosphere. The physical mechanism for the energy transfer from the solar wind to the magnetosphere is magnetic reconnection between the interplanetary magnetic structure and the Earth's magnetic field (e.g. Gonzalez, 1994). The scenario of magnetic reconnection was first proposed by Dungey (1961) (see also Tsurutani et al., 2019, and references therein) and is schematically shown in Figure 5.1. If the interplanetary magnetic field has southward component, it will interconnect with the Earth's magnetopause northward magnetic field. The solar wind drags the interconnected magnetic fields and plasma downstream (in the antisunward direction). The open magnetic fields then reconnect in the tail. Reconnection leads to a strong convection of the plasma sheet into the night-side magnetosphere. Intense southward IP magnetic fields drive intense magnetic reconnection at the day-side magnetopause and intense reconnection on the night-side, thus leading to intense geomagnetic storms.

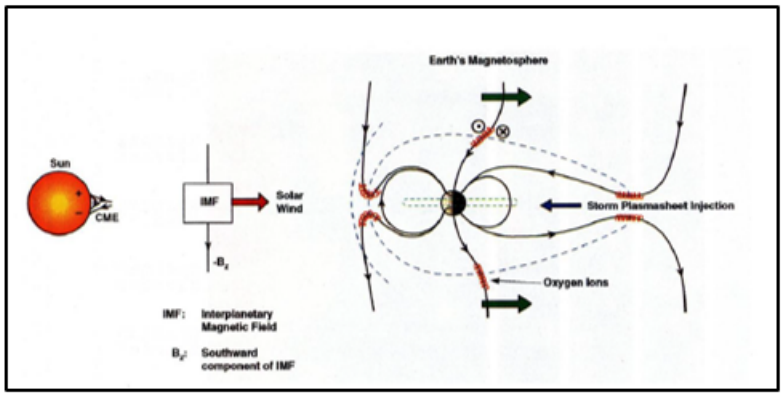


Figure 5.1: Schematic diagram of magnetic reconnection powering geomagnetic storms (Tsurutani et al. (2019) updated from Dungey (1961)).

## 5.4 Dependence of Storm Strengths on their Source Characteristics

The properties of geomagnetic storms and their dependence on the IP structures and solar wind parameters have been widely studied. Weak and moderate storms can be caused by both ICMEs and CIRs (e.g. Xu et al., 2009; Yakovchouk et al., 2012), while the more intense storms are mostly caused by CME-driven IP disturbances (e.g. Zhang et al., 2007; Richardson & Cane, 2012). Only about 10–15 % of the intense storms are due to CIRs and the corresponding Dst index is close to $-100$ nT (e.g. Zhang et al., 2007; Richardson et al., 2006). Richardson et al. (2006) estimated that the upper limit on CIR-associated storms is likely to be Dst $\sim -180$ nT, and concluded that CIRs are unlikely to be a source of severe storms. Obridko et al. (2013) found that storms with sudden commencements are caused by ICMEs while storms with gradual commencements are associated with HSS from coronal holes. Xu et al. (2009) found that geomagnetic storms in solar cycle 23 did not strictly keep in line with the sunspot number, and concluded that Earth's upstream solar wind conditions played a key role in solar-terrestrial coupling. However, most severe storms occur during the maximum phase of the solar cycle, and they are primarily associated with ICMEs (e.g. Zhang et al., 2007).

The behavior of the Dst index can be explained by the integrated $B_s$ and the y-component (in the geocentric solar ecliptic reference frame) of the solar wind electric field ($E_y \sim V_{sw}.B_s$, where $V_{sw}$ is the solar wind speed ) (e.g. Echer et al., 2008; Richardson & Cane, 2010). In a study of intense storms in solar cycle 23, Zhang et al. (2007) found that the intense storms might be caused by three different IP structures: 60 % of all storms were caused by a single ICME originated from a single CME, 27 % were caused by multiple interacting ICMEs arising from multiple halo CMEs launched from the Sun in a short period, and only 13 % were caused by CIRs. Xu et al. (2009) found

that 60 % of intense storms were totally induced by shock-driving magnetic clouds. They showed that shock-driving magnetic clouds were most geoeffective interplanetary sources with ∼4/5 (81 %) of them able to lead to storms with Dst $\leq -30$ nT and more than 1/3 (36 %) to intense storms. In a subsequent study of storms with Dst $\leq -200$ nT, Szajko et al. (2013) found that ∼1/3 of storms were caused by ICME-magnetic clouds, ∼1/3 by sheath fields, and ∼1/3 by combined sheath and ICME-magnetic cloud fields. In a recent study, Gopalswamy et al. (2015) found that the product of the magnetic cloud flow speed and the southward component of the cloud magnetic field was the primary factor determining the strength of geomagnetic storms.

## 5.5 Geoeffectiveness of CMEs

The geoeffectiveness of CMEs refer to the ability of CME-driven IP magnetic structures in causing geomagnetic storms. Based on the Dst index, CMEs are described as weakly, moderately, and strongly geoeffective if they produce geomagnetic storms with $-50$ nT $<$ Dst $\leq -30$ nT, $-100$ nT $<$ Dst $\leq -50$ nT, and Dst $\leq -100$ nT, respectively. In general, a CME is defined as geoeffective if it is followed by a storm with Dst $\leq -50$ nT (e.g. Gopalswamy et al., 2007, and references therein). Several CME parameters have been proposed as important parameters of geoeffective CMEs: angular width, location, speed, earthward direction, and IP magnetic field direction.

The front-side (location on the visible disk) halo (angular width $\geq$120°) CMEs presumably propagating along the Sun–Earth line are the most probable candidates to be geoeffective. However, only a small portion of these CMEs causes geomagnetic activity because either they are not actually directed towards the Earth, or their interplanetary counterparts do not posses sufficient southward magnetic field regions (e.g. Cane et al., 2000; Webb et al., 2000; Wang et al., 2002; Zhang et al., 2003; Zhao & Webb, 2003; Kim et al., 2005; Gopalswamy et al., 2007). Wang et al. (2002) found that the source locations of geoeffective halo CMEs had a western bias due to the solar magnetic field spiral structure (see also, Zhang et al., 2003). Zhao & Webb (2003) found that during the early ascending phase of the solar cycle 23 nearly all halo CMEs were geoeffective, but towards the solar cycle maximum the rate of geoeffectiveness reduced to 40 %. They suggested that the origin of the CMEs from source regions under the bipolar coronal streamer belt at the base of the heliospheric current sheet lead to a weaker chance of generating sustained southward magnetic field structures at 1 AU due to increased inclination of the heliospheric current sheet during solar maximum. In a comprehensive study of the geoeffectiveness of 378 halo CMEs in solar cycle 23 Gopalswamy et al. (2007) found that the overall strength of the storms declines as the solar source location changes from the disk to limb to backside. The disk halos (longitudinal distance from the disk centre $\leq$ 45 degree) were strongly geoeffective and the limb halos were moderately geoeffective, while the backside halos were not followed by significant storms. Source location and speed of the CMEs were the most important parameters explaining geoeffectiveness, while there was no significant difference in the flare size among geoeffective and nongeoeffective halo CMEs.

Srivastava & Venkatakrishnan (2004) showed that a large percentage (62 %) of the

geoeffective CMEs are faster than 700 km s$^{-1}$. Dumbović et al. (2015) concluded that faster CMEs had higher probability of producing strong geomagnetic storms and slow CMEs ($< 600$ kms$^{-1}$) were not likely to produce very intense (Dst $\leq -200$ nT) storms, unless involved in interaction with a faster CME. The correlation coefficients between the linear sky-plane speed of CMEs and the strength of the associated geomagnetic storms are relatively good and ranging from $\sim -0.45$ to $\sim -0.65$ (e.g. Srivastava & Venkatakrishnan, 2004; Gopalswamy, 2010a; Vasanth & Umapathy, 2013; Shanmugaraju et al., 2015). Michalek (2006) and Michalek et al. (2007) showed that the correlation between the storm strength and space speed of the CME is stronger compared to that of the projected sky-plane speed. They also showed that the correlation between the storm strength and both the sky-plane and space speed of the CMEs for the western events is significantly stronger compared to those of the eastern events.

The earthward-direction parameter (DP) of CMEs has been proposed as a new important geoeffectiveness parameter of CMEs (Moon et al., 2005). The direction parameter quantifies the symmetric characteristics of a CME seen in a coronagraph image and it is used to estimate the propagation direction of front-side halo CMEs. Kim et al. (2008) used this parameter in studying the geoeffectiveness of 486 front-side halo CMEs and showed that CMEs with large direction parameters had a high association with geomagnetic storms. With increasing direction parameter, the geoeffectiveness also increased. Kim et al. (2010) and Shanmugaraju et al. (2015) have found relatively good correlations between DP and the Dst index (0.60 and 0.57, respectively). On the other hand, the southward orientation of the magnetic field in the CME source region may play the most important role in the production of geomagnetic storms (e.g. Kang et al., 2006; Lee et al., 2014, and references therein).

## 5.6 Prediction of Geomagnetic Storms

Prediction of the occurrence and strength of geomagnetic storms is a highly important issue for space weather applications. The occurrence of geomagnetic storms can be predicted qualitatively, when large events on the Sun, such as CMEs or coronal holes, are detected. The solar wind associated with these solar events takes about 1-5 days to propagate from the Sun to the Earth, creating the natural time interval for such predictions. However, their IP magnetic structure parameters observed by spacecraft at the Lagrange L1 point are also very important for such predictions. Based on the warning time, there are two main groups of forecast models: long-term (order of days) and short-term ($\lesssim$ 1 hours). Many authors have proposed forecast models with varying success rates and reliability. Long-term forecast models are based on the observed CME parameters at the Sun (e.g. Kim et al., 2010; Shanmugaraju et al., 2015, and references therein), while short-term forecast models are based on the measurements of the solar wind parameters and magnetic fields at the Lagrange L1 point 1.5 million kilometres from the Earth towards the Sun (e.g. Temerin & Li, 2002, 2006; Ji et al., 2012; Podladchikova et al., 2018, and references therein).

Kim et al. (2010) proposed a storm strength prediction formula, which in the case of the observed southward magnetic field orientation included the CME direction pa-

rameter and the CME speed as independent variables, and for the northward events the CME source locations as the third independent variable. For their southward and northward models they found correlation coefficients with Dst minimum of 0.66 and 0.80, respectively. By using the real-time solar wind data, Ji et al. (2012) compared six Dst forecast models using 63 intense geomagnetic storms and they found that the forecast model by Temerin & Li (2002, 2006) gives the best prediction of real-time Dst. Ji et al. (2012) found that the correlation coefficient and the root-mean-square errors between the observed Dst and the predicted Dst calculated by the forecasting model of Temerin & Li (2002, 2006) during the time period of the geomagnetic storm were 0.94, and 14.8 nT, respectively. They also found that the difference between the value and the time of the observed minimum Dst and the predicted minimum Dst were 7.7 nT, and 1.5 hours, respectively. Although the short-term forecasts are more reliable than the long-term forecasts, they suffer from the very short ($\lesssim$ 1 h) warning time.

Since the ESP events are associated with IP shocks driven by CMEs, they can be used as a warning of a disturbance approaching the Earth. Some studies (e.g. Smith et al., 2004; Valtonen et al., 2005; Lam, 2009; Le et al., 2016) have proposed that ESPs could be used for mid-term (hours to a day) forecasting of geomagnetic storms. Smith et al. (2004) evaluated possibilities of using energetic ion enhancements in forecasting geomagnetic storms. They found that most (95 %) of the energetic ion enhancements with maximum flux $> 10^5$ cm$^{-2}$s$^{-1}$sr$^{-1}$MeV$^{-1}$ were followed by geomagnetic activity with $K_p > 4$ and 80 % by storms with $K_p > 5$. Lam (2009) showed that the maximum geomagnetic activity is related to the maximum particle enhancements in a non-linear fashion. By using the time differences between the SEP and ESP observations related to the same CME Valtonen et al. (2005) demonstrated the feasibility of such observations in evaluating geoeffectiveness of halo CMEs. Recently Le et al. (2016) suggested that SEP intensity-time profiles can be classified in three types with the CMEs associated with each type having different geoeffectiveness.

# Chapter 6

# Summary of the Original Publications

## 6.1 Article I

**Investigation of the Geoeffectiveness of Disk-Centre Full-Halo Coronal Mass Ejections**

We investigated the occurrence and the strength of geomagnetic storms associated with disk-centre full-halo coronal mass ejections (DC-FH-CMEs) during the Solar Cycles (SCs) 23 and 24. Such CMEs can be considered as the most plausible causes of geomagnetic storms.

The aim was to study the dependence of the occurrence and strength of geomagnetic storms on the parameters characterizing the CMEs and their interplanetary counterparts in different phases of solar cycles, and the differences between SC 23 and 24

The Large Angle and Spectrometric Coronagraph on board SOHO (SOHO/LASCO) (Brueckner et al., 1995) was used to select the CME data. Dst index from the World Data Center for Geomagnetism, Kyoto, was used to characterise the strength of the geomagnetic storms. The solar wind conditions at the time of the geomagnetic storms at 1 AU were examined by using the OMNI database of the Space Physics Data Facility at Goddard Space Flight Center.

We selected the full-halo CMEs from the SOHO/LASCO catalogue from the beginning of 1996 till the end of 2015 with source locations between solar longitudes E10 and W10 and latitudes N20 and S20. We found 66 DC-FH-CMEs fulfilling the selection criteria. We associated the DC-FH-CMEs with geomagnetic storms by estimating the arrival times of the corresponding interplanetary CMEs at 1 AU using the drag-based model (Vršnak *et al.*, 2013). The basic CME-storm association criterion was that a geomagnetic storm with minimum Dst $\leq -50$ nT occurred within a $\pm 24$ h time window from the predicted arrival time of the ICME.

Thirty-three of the 66 DC-FH-CMEs (50 %) were deduced to be the cause of 30 geomagnetic storms with Dst $\leq -50$ nT. Thirteen of the 66 DC-FH-CMEs were associated with 13 (20 %) moderate storms and were described as moderately geoeffective, while 20 (30 %) were strongly geoeffective associated with 17 strong storms. We found only a weak correlation between the minimum Dst of the geomagnetic storms and the

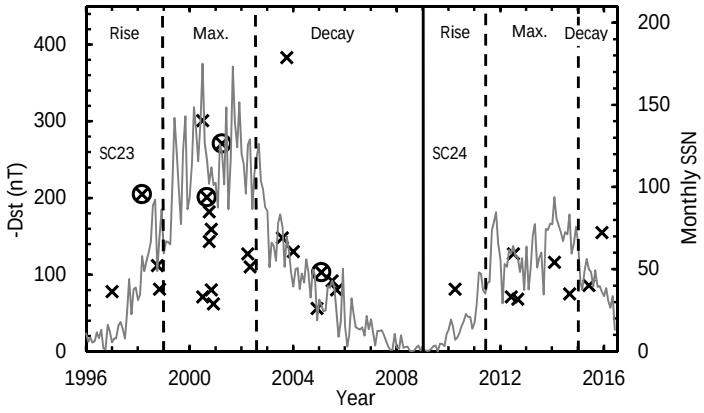


Figure 6.1: Time dependence of the strength of the geomagnetic storms caused by the DC-FH-CMEs. The crosses represent the storms with Dst minimum values $\leq -50$ nT. The crosses surrounded by circles represent storms associated with multiple CMEs. For comparison, the monthly average sunspot number is also shown. The vertical line separates Solar Cycles 23 and 24 and the dashed lines separate various phases of the cycles.

CME sky-plane speed ($-0.42$) and the CME direction parameter ($-0.31$), while the correlation was strong between the Dst and all the solar wind parameters measured at 1 AU. The correlation coefficients between the Dst index and solar wind parameters were $-0.76$ for the total magnetic field strength ($B_t$), $-0.77$ for the southward component of the magnetic field, $-0.73$ for the solar wind speed, and $-0.87$ for the y-component of the solar wind electric field.

In the rise phase of SC 23 there were several DC-FH-CMEs and they had a high rate of geoeffectiveness (63 %), while in the rise phase of SC 24 there were only few events, one of them moderately geoeffective (the geoeffectiveness rate of 25 %) with Dst of $-81$ nT. At the maximum phases of the cycles 23 and 24 the largest number of DC-FH-CMEs (21 and 17 events, respectively) occurred. The rate of geoeffectiveness was high (62 %) for the maximum phase of SC 23, but low (29 %) for SC 24. Most of the storms with Dst $\leq -100$ nT occurred at or close to the maximum phases of the cycles (see Figure 6.1).

We examined the properties of DC-FH-CMEs, associated solar wind parameters, and geomagnetic storms during the first 85 months of SCs 23 and 24. The average sunspot number in SC24 declined by 46.5 % compared to SC 23. There was a large reduction in the number of geoeffective DC-FH-CMEs (56 %), which is significantly larger than the decline in the number of all DC-FH-CMEs (26 %) and the reduction in the average initial speed (13 %) and direction parameter (12 %) of all DC-FH-CMEs. The reduction in the solar wind parameters $B_t$ (26 %), $B_s$ (31 %), and $E_y$ (39 %) were

also large. The changes in the geoeffectiveness rate of DC-FH-CMEs ($-40\,\%$) and in the average Dst of geoeffective DC-FH-CMEs ($-34\,\%$) from SC 23 to SC 24 were the consequences of the lower $B_s$ and $E_y$ of the disturbances encountering Earth during SC 24.

## 6.2 Article II

**Potential Role of Energetic Particle Observations in Geomagnetic Storm Forecasting**

The topic of the article was the occurrence and strength of geomagnetic storms caused by CMEs associated with proton events consisting of both SEPs accelerated near the Sun and ESPs accelerated by interplanetary shocks driven by the CMEs and observed near the time when the shock passed the observer. We also studied the relationships between the strength of geomagnetic storms (Dst index) and parameters characterizing the SEPs, ESPs, CMEs, and solar flares.

The aim was to investigate the possibilities and advantages of using energetic particle observations for mid-term (warning time several hours) forecasting of geomagnetic storms or as a support for longer-term forecasting methods based on solar observations.

The Energetic and Relativistic Nuclei and Electron experiment (ERNE) aboard the SOHO (Torsti *et al.*, 1995), and the instruments aboard the Geostationary Operational Environmental Satellites (GOES) were used to select the proton data. ERNE consists of two detectors, Low Energy Detector (LED) and High Energy Detector (HED) with several differential energy channels covering the ranges 1.3 – 14 MeV for LED and 13 – 140 MeV for HED with one minute time resolution. The GOES satellites also have two detectors, Energetic Particle Sensor (EPS) and High energy Proton and Alpha Detector (HEPAD). The integral and differential energy channels cover the ranges 0.6 – 500 MeV for EPS and from 350 MeV to $>700$ MeV for HEPAD with 5 minute time resolution. The occurrence times of the interplanetary shocks were found from the SOHO/CELIAS observations and the interplanetary shock database of the Advanced Composition Explorer and the Wind spacecraft. SOHO/LASCO and GOES soft X-ray data were used to identify the CMEs and solar flares, respectively. The Kyoto Dst data were used to characterise the strength of the geomagnetic storms.

We searched for SEP and ESP events through the time period 1996 – 2017 by using the proton data from ERNE (or GOES during the data gaps of ERNE) at two energies, 2 MeV (1.78 – 2.16 MeV) and 20 MeV (16.9 – 26 MeV). In general, the SEP events were associated with fast ($>400\,\mathrm{km\,s^{-1}}$) and wide ($>60^\circ$) CMEs closest in time to the onsets of the SEP events at 20 MeV. To associate CMEs, and thus the SEP and ESP events, with the geomagnetic storms we used the same method as in Article I.

We identified altogether 95 SEP–ESP events at 2 MeV or 20 MeV proton energies for which it was possible to determine the SEP onset time, ESP peak time, and CME association. We found that 65 out of the 95 ($68\,\%$) SEP–ESP events were associated with geomagnetic storms with minimum Dst $\leq -50$ nT caused by CMEs, while the rest 30 events were not associated with geomagnetic storms or were associated with only weak geomagnetic activity (Dst $> -50$ nT). Twenty-four of the 65 SEP–ESP events

were associated with moderate storms ($-100\,\mathrm{nT} < \mathrm{Dst} \leq -50\,\mathrm{nT}$) and 41 with strong storms ($\mathrm{Dst} \leq 100\,\mathrm{nT}$).

We also found 45 events consisting of only SEPs and 10 events of only ESPs associated with geomagnetic storms caused by CMEs. In addition, we identified 139 SEP events at 20 MeV which were not associated with geomagnetic storms. The average minimum Dst of geomagnetic storms associated with the SEP–ESP events was significantly lower than those of storms associated with the other types of particle events.

When comparing characteristics of solar events associated with geomagnetic storms but lacking energetic protons we found that in this group the average CME speed and the flare flux were lower, the source location was further from the magnetically well connected region, and the association with decametric-hectometric type II radio bursts was weaker than in the group also associated with energetic proton events. Thus, solar events of the first group tend to be too weak to be efficient particle accelerators or in some cases originate from solar regions from which energetic particles do not easily reach the Earth. For events associated with energetic particles, the CME direction parameter and the angular distance of the source region from the solar disk centre were the differentiating factors between the CMEs not causing storms and those leading to storms.

For the 65 storm-associated SEP – ESP events we studied the correlations between several parameters characterizing the particle events and the associated solar phenomena and the minimum value of the Dst index during the storms. For a single independent explaining variable we found that the best correlations were between the logarithm of the absolute value of the minimum Dst and the difference between the ESP peak time and the onset time of the associated SEP event ($\triangle \mathrm{t}_{ESP-SEP}$) or CME direction parameter (DP). To improve the correlation, we investigated combinations of various parameters. The best correlation for two independent variables was obtained for the combination of $\triangle \mathrm{t}_{ESP-SEP}$ and DP at 2 MeV. The correlation slightly improved when adding a third independent variable, the logarithm of the maximum energy of ESPs. As the final result of the article we suggested a formula based on these three parameters for estimating the minimum Dst. Using this method the average warning time for geomagnetic storms was found to be $(15 \pm 10)$ hours.

## 6.3 Article III

**Solar Energetic Particle Events Related to Disk-Centre Full-Halo Coronal Mass Ejections.**

The aim of this article was to study the occurrence rate of solar energetic particle events related to full-halo coronal mass ejections originating from the disk centre of the Sun, and to study the correlations between the SEP peak intensities at different energy ranges with parameters characterizing their solar sources.

The SOHO/LASCO catalog of full halo CMEs was used to select the events. The GOES soft X-ray data were used to identify the source locations and the peak fluxes of soft X-rays. The SOHO/ERNE data were used for the proton intensities.

Table 6.1: The correlation coefficients between the SEP peak intensities in three energy channels and the CME speeds and the solar flare peak and integrated fluxes

| Parameter | 2 MeV | 20 MeV | 68 MeV |
|---|---|---|---|
| CME sky-plane speed | 0.68 | 0.82 | 0.47 |
| CME space speed | 0.71 | 0.83 | 0.47 |
| X-ray flare peak flux | 0.63 | 0.85 | 0.88 |
| X-ray flare integrated flux | 0.86 | 0.89 | 0.64 |

For this investigation we selected full-halo CMEs from 1996 till the end of 2014 with the source locations between solar longitudes E10 and W10 and latitudes N20 and S20. We found altogether 64 events. Based on the solar latitude, we divided the selected events in three subgroups: 26 (41 %) equatorial events in the latitude range [N10, S10], 16 (25 %) northern events in the range (N10, N20], and 22 (34 %) southern events in the range (S10, S20].

We searched for the ERNE proton data at three energy channels 1.33 – 2.66 MeV (nominal energy 2 MeV), 13.8 – 29.0 MeV (20 MeV), and 50.8 – 86.7 MeV (68 MeV) to find out solar proton events associated with the selected CMEs. In 25 (39 %) cases an association between the CMEs and the SEP events was found at least in one energy channel. Because no significant difference was found for the SEP events association with the CMEs from the three solar latitude regions, all events were combined for the correlation studies.

We found statistically significant correlations between the proton peak intensities in the three energy channels with the CME speeds and with the X-ray flare peak flux and integrated flux (see Table 6.1). The weakest correlations were found at the highest proton energy for all parameters except for the X-ray peak flux.

## 6.4 Article IV

**Properties of High-Energy Solar Particle Events Associated with Solar Radio Emissions.**

We analysed 58 high-energy solar proton events and 36 temporally related near-relativistic electron events for which the velocity dispersion analysis of the first-arriving particles gave the apparent path lengths between 1 and 3 AU.

The aim of this article was to study the dependence of the characteristics of the proton events, the related electron events, and their solar sources, on the associations of type II, III, and IV radio bursts.

Proton data from SOHO/ERNE and electron data from the 3-D Plasma and Energetic Particle Investigation (3DP) spectroscopic survey telescopes on board the Wind spacecraft (Lin *et al.*, 1995) were used in the analysis. SOHO/LASCO observations of the CMEs associated with the SEP events were used, and GOES soft X-ray data were used to identify the source locations and the characteristics of the soft X-ray flares. The Wind/Plasma and Radio Waves (WAVES) data (Bougeret et al., 1995) were searched

for type III radio bursts associated with the selected proton events. The decametric-hectometric (DH) type II and type IV radio bursts associated with the events were identified from the lists compiled by the Wind and STEREO data center. The metric type II and type IV radio burst data were obtained from several different ground-based stations, such as the Radio Solar Telescope Network, Hiraiso Radio Spectrograph, Green Bank Solar Radio Burst Spectrometer, Bruny Island Radio Spectrometer, and Nancay Decameter Array.

From a list of high-energy (55 – 80 MeV) proton events during the years 1996 – 2016, we selected 58 events for which the velocity dispersion analysis of the first-arriving particles gave the apparent path lengths between 1 and 3 AU. We then searched for electron events temporally related with these 58 proton events. With the same criterion for the path length as for protons, we found 36 electron events.

We found that all proton events were associated with decametric type III radio bursts. Almost all proton events (56/58) were associated with type II radio bursts. Eleven of these 56 type II bursts were observed at metric wavelengths only, 11 at DH only, and 34 at both wavelength ranges. Some of the events (32/58) were associated with metric type IV radio bursts while no events were associated with DH type IV bursts.

In 19 of the 36 temporally related electron and proton events protons were released simultaneously (within $\pm$7 minutes) with the electrons, in 16 events protons were released later than the electrons, and in one event electrons were released after the protons.

Electron release times with respect to radio type III onsets were similar in all events, but in events where the protons were released after the electrons also the differences between the proton release times and type III onsets were significantly larger than in simultaneous proton and electron events. This indicates that the proton release times in the delayed events were not only later than those of the electrons, but they were also more delayed with respect to the decametric type III emission.

Based on the wavelength range of the associated type II radio emission and the temporal relation of the proton release with respect to the type II onset we divided the 56 proton events into two categories. In Category 1 are the events which were associated with only metric type II emission or both m and DH type II and the release time of protons was before the DH type II onset (18/56 events). Category 2 consists of the events which were associated with only DH type II emission or both m and DH type II and the protons were released at or after the DH type II onset (31/56 events). For seven of the 56 events we were not able to determine a definite category due to timing uncertainties. The characteristics of the particle events and the properties of the associated CMEs and solar flares in the two categories were significantly different.

1. On average Category 1 events had significantly smaller time differences between the proton release times and the radio type III onsets than Category 2 events. In almost all Category 1 events (83 %) proton release occurred during the type III emission.

2. In Category 1 events the angular distances from the magnetic footpoint leading to Earth were small, while Category 2 events were more scattered in the connection angle, many events with large negative angles.

3. Proton release heights at the Sun were estimated by using the CME height-time extrapolation and the atmospheric electron density model. On average Category 1 events had significantly lower proton release heights than Category 2 events.

4. The proton intensity rise rate of Category 1 events was significantly higher than that of Category 2 events. On average Category 1 events had significantly smaller intensity rise times than Category 2 events, while the maximum intensities were not significantly different between the two categories. There was a strong correlation between the proton intensity rise rate and both the time difference between the proton release time and the type III onset and the proton release height.

5. There was quite significant overlap of the proton spectral indices in the two categories, but on average Category 1 events had harder spectra than Category 2 events.

6. The average rise time and duration of the soft X-ray flares associated with Category 1 events were significantly shorter than those of Category 2 events while the average peak flux did not significantly differ. In 65 % of Category 1 events, the proton release time was before or within uncertainties coincident with the X-ray peak time, while in 77 % of Category 2 events it was after the X-ray peak time.

7. There were no significant differences in the average CME sky-plane speed between the Category 1 and Category 2 events, whereas the CME average width in Category 1 events was smaller than in Category 2 events. The average initial CME accelerations in Category 1 and Category 2 events were not statistically significantly different.

8. The simultaneous proton and electron events and the delayed proton events did not unambiguously fall in the two categories of proton events, although most of the events in which the protons were released after the electrons belonged to Category 2.

# Chapter 7

# Conclusions

Solar energetic particles (SEPs) and geomagnetic storms are important manifestations of space weather which can affect technologies used by modern society both in space and on ground.

In this thesis we have investigated the properties of solar energetic particles and geomagnetic storms caused by coronal mass ejections (CMEs). We have studied the occurrence and strength of SEP events and geomagnetic storms and their dependence on the parameters characterizing coronal mass ejections and other solar phenomena, such as solar flares and solar radio bursts, temporally related to the CMEs.

We investigated the geoeffectiveness of full-halo CMEs originating from the solar disk centre during the last two solar cycles by using coronagraph observations of SOHO/LASCO and solar wind measurements from the NASA OMNI database. The temporal association of the observed CMEs with the geomagnetic storms was performed by using a drag-based model describing the propagation of the CMEs in the interplanetary space and arrival at Earth. Half of the CMEs were found to generate geomagnetic storms. The strength of the geomagnetic storms best correlated with the solar wind parameters, while there was only a weak dependence on the CME speed and on a parameter describing the propagation direction of the CME. The occurrence rate and the strength of the geomagnetic storms were dependent on the solar activity cycle (solar cycles 23 and 24) and on the phase of the cycle. During the current solar cycle 24, the number of geoeffective disk-centre full-halo CMEs was less than half of that during cycle 23.

We also investigated the association of the disk-centre full-halo CMEs with solar particle events. Good correlations were found between the proton event peak intensity and both the CME speed and the solar soft X-ray flare magnitude. The correlations were dependent on the particle energies.

We studied the feasibility of using energetic particle measurements together with coronal mass ejection observations for geomagnetic storm forecasting. We found that almost 70 % of the proton events consisting of solar energetic particles accelerated near the Sun and energetic storm particles (ESPs) accelerated by interplanetary shocks driven by CMEs and observed near the Earth were associated with geomagnetic storms. We proposed an empirical formula for the storm strength forecasting, in which the explaining parameters are the difference between the observed ESP peak time and the onset

time of the associated SEP event, the maximum energy of the ESPs, and a parameter describing the propagation direction of the CME. This formula can be used for mid-term forecasting of geomagnetic storm strengths providing a warning time of (15 $\pm$10) hours.

Using SOHO/ERNE measurements of high-energy protons, Wind/3DP measurements of near-relativistic electrons, and solar radio observations from several ground stations and by Wind/WAVES in space, we performed an analysis of the associations of high-energy solar particle events with solar radio type II, III, and IV bursts and of the release times of the particles with respect to these bursts. We discovered that the proton events can be divided into two categories. The distinctive factors between the categories were the wavelength range of the associated type II radio emission and the temporal relation of the proton release with respect to the type II burst onset. The characteristics of the proton events in the Categories 1 and 2 were statistically significantly different. We concluded that protons in Category 2 events were accelerated by CME-driven shocks high in the solar corona. In Category 1 events, protons were accelerated low in the corona either by CME shocks or in flare or CME-initiation related processes. We further concluded that in about half of the events protons and electrons were released and presumably also accelerated simultaneously within $\pm$7 minutes. In the rest of the events proton release was delayed with respect to electrons, with the exception of one event in which electrons were released later than protons. The cause of the delays remained unclear.

# Bibliography


Antalova, A.: 1985, *Contributions of the Astronomical Observatory Skalnate Pleso*, **13**, 243

Antiochos, S. K., Devore, C. R., Klimchuk, J. A.: 1999, *The Astrophysical Journal*, **510**, 485

Baker, D.N.: 2000, *IEEE Transactions on Plasma Science*, **28**, 2007

Bąk-Stęślicka, U. and Kołomański, S., Mrozek, T.: 2013, *Solar Physics* **283**, 505

Bala, B., Lanzerotti, L. J., Gary, D. E., Thomson, D. J.: 2002, *Radio Science*, **37**, 1018

Barbieri, L. P., Mahmot, R. E.: 2004, *Space Weather*, **2**, S09002

Bartels, J., Heck, N. H., Johnston, H. F.: 1939, *Journal of Geophysical Research*, **44**, 411

Bastian, T.S., Pick, M., Kerdraon, A., Maia, D., Vourlidas, A.: 2001, *The Astrophysical Journal*, **558**, L65.

Benz, A.O.: 1980, *The Astrophysical Journal*, **240**, 892

Boischot, A., Riddle, A. C., Pearce, J. B., Warwick, J. W.: 1980, *Solar Physics*, **65**, 397

Bolduc L.: 2002, *Journal of Atmospheric and Solar-Terrestrial Physics*, **64**, 1793

Bothmer, V., Zhukov, A.: 2007, The Sun as the prime source of the space weather, in: Space Weather-Physics and Effects, Springer Praxis Books, Berlin, 31

Bougeret, J. L.: 1985, in: Collisionless shocks in the heliosphere, (eds.) Tsurutani, B.T., Stone, R.G., *AGU, Geophysical Monograph Series*, **34**, 13

Bougeret, J. L., Kaiser, M.L., Kellogg, P.J., Manning, R., Goetz, K., et al.: 1995, *Space Science Reviews*, **71**, 231

Bougeret, J. L., Zarka, P., Caroubalos, C., Karlický, M., Leblanc, Y., et al.: 1998, *Geophysical Research Letters*, **25**, 2513.

Brueckner, G.E., Howard, R.A., Koomen, M.J., Korendyke, C.M., Michels, D.J., et al.: 1995, *Solar Physics*, **162**, 357.

Bryant, D. A., Cline, T. L., Desai, U. D., McDonald, F. B.: 1962, *Journal of Geophysical Research*, **67**, 4983

Burkepile, J.T., Hundhausen, A.J., Stanger, A.L., St. Cyr, O.C., Seiden, J.A.: 2004, *Journal of Geophysical Research*, **109**, A03103.

Burlaga, L. F., Chao, J. K.: 1971, *Journal of Geophysical Research*, **76**, 7516

Cairns, I. H., Knock, S. A., Robinson, P. A., Kuncic, Z.: 2003, Type II Solar Radio Bursts: Theory and Space Weather Implications. In: Chian A.CL. et al. (eds) Advances in Space Environment Research. Springer, Dordrecht, 27

Cane, H.V., Stone, R.G., Fainberg, J., Stewart, R.T., Steinberg, J.L., and Hoang, S.: 1981, *Geophysical Research Letters*, **8**, 1285

Cane, H. V., Stone, R. G., Fainberg, J., Steinberg, J. L., Hoang, S.: 1982, *Solar Physics*, **78**, 187

Cane, H. V., Stone, R. G.: 1984, *The Astrophysical Journal*, **282**, 339

Cane, H. V.: 1995, *Nuclear Physics B - Proceedings Supplements*, **39**, 35

Cane, H. V., Richardson, I. G., Wibberenz, G.: 1997, *Journal of Geophysical Research*, **102**, 7075

Cane, H. V., Richardson, I. G., Cyr, O. C. St.: 2000, *Geophysical Research Letters*, **27**, 3591

Cane, H. V., Erickson, W. C.: 2005, *The Astrophysical Journal*, **623**, 1180

Cane, H. V., Richardson, I.G., von Rosenvinge, T.T.: 2010, *Journal of Geophysical Research*, **115**, A08101

Carrington, R. C.: 1859, *Monthly Notices of the Royal Astronomical Society*, **20**, 13

Chen, Y., Song, H. Q., Li, B., Xia, L. D., Wu, Z., Fu, H., Li, X.: 2010, *The Astrophysical Journal*, **714**, 644

Chen, Y., Feng, S. W., Li, B., Song, H. Q., Xia, L. D., Kong, X. L., Xing Li.: 2011, *The Astrophysical Journal*, **728**, 147

Chen, Y., Du, G., Feng, L,. Feng, S., Kong, X., Guo, F., Wang, B., Li, G.: 2014, *The Astrophysical Journal*, **787**, 59

Cheng, X., Ding, M. D., Zhang, J., Sun, X. D., Guo Y., Wang, Y. M., Kliem, B., Deng, Y. Y.: 2014, *The Astrophysical Journal*, **789**, 93

Cho, K. -S., Bong, S. -C., Moon, Y. -J., Shanmugaraju, A., Kwon, R. -Y., Park, Y. D.: 2011, *Astronomy and Astrophysics* **530**, A16

Cliver, E. W., Ling, A. G.: 2009, *The Astrophysical Journal*, **690**, 598

Cliver, E. W., Webb, D. F., Howard, R. A.: 1999, *Solar Physics*, **187**, 89

Cliver, E. W., Kahler, S. W., Reames, D. V.: 2004, *The Astrophysical Journal*, **605**, 902

Cliver, E. W., Ling, A. G., Belov, A., Yashiro, S.: 2012, *The Astrophysical Journal Letters*, **756**, L29

Cliver, E.W.: 2000, In AIP Conference Proceeding 528, Acceleration and transport of energetic particles observed in the heliosphere, (eds.) Mewaldt, R. A., Jokipii, J. R., Lee, M. A., et al., New York, AIP, 21

Cohen, C. M. S.: 2006, in: Solar Eruption and Energetic Particles, (eds.) Gopalswamy, N., Mewaldt, R., Torsti, J., *AGU, Geophysical Monograph Series*, **165**, 275

Daly, E., Glover, A., Hilgers, A.: 2007, Effects on Spacecraft Hardware and Operation, in: Space Weather-Physics and Effects, Springer Praxis Books, Berlin, 353

Decker, R. B.: 1988, *Space Science Reviews*, **48**, 195

Dennis, B. R.: 1988, *Solar Physics*, **118**, 49

Desai, M., Giacalone, J.: 2016, *Living Reviews in Solar Physics*, **13**, 3

Dierckxsens, M., Tziotziou, K., Dalla, S., Patsou, I., Marsh, M. S., Crosby, N. B., Malandraki, O., Tsiropoula, G.: 2015, *Solar Physics*, **290**, 841

Dodd, P. E., Massengill, L. W.: 2003, *IEEE Transactions on nuclear Science*, **50**, 583

Dumbović, M., Devos, A., Vršnak, B., Sudar, D., Rodriguez, L., Ruždjak, D., Leer, K., Vennerstrøm, S., Veronig, A.: 2015, *Solar Physics* **290**, 579

Dungey, J. W.: 1961, *Physical Review Letters*, **6**, 47

Echer, E., Gonzalez, W. D., Tsurutani, B. T.: 2008, *Geophysical Research Letters*, **35**, L06S03

European Cooperation for Space Standardization: 2008, ESA Requirements and Standards Division, ECSS-E-ST-10-04C

Elgaroy, E. O.: 1977, Solar Noise Storms, Oxford, Pergamon Press, London.

Estienne, J. P.: 1993, Space Environment and EMC/ESD Phenomena. In: The Behavior of Systems in the Space Environment. (eds.) DeWitt R. N., Duston D., Hyder A. K., NATO ASI Series, Dordrecht, **245**, 513

Evans, R. M., Opher, M., Gombosi, T. I.: 2011, *The Astrophysical Journal*, **728**, 41

Fainberg, J., Stone, R. G.: 1970, *Solar Physics*, **15**, 222

Feng, S. W., Chen, Y., Li, B., Song, H. Q., Kong, X. L., Xia, L. D., Feng, X. S.: 2011, *Solar Physics* **272**, 119

Forbush, S. E.: 1946, *Physical Review*, **70**, 771

Forman, M. A., Webb, G. M.: 1985, in: Collisionless shocks in the heliosphere, (eds.) Tsurutani, B.T., Stone, R.G., *AGU, Geophysical Monograph Series*, **34**, 91

Gallagher, P. T., Lawrence, G. R., Dennis, B. R.: 2003, *The Astrophysical Journal Letters*, **588**, L53

Gilbert, H. R., Holzer, T. E., Burkepile, J. T., Hundhausen, A. J.: 2000, *The Astrophysical Journal*, **537**, 503

Ginzbursg, V. L., Zheleznakov, V. V.: 1958, *Soviet Astronomy Journal*, **2**, 653

Gonzalez, W. D., Joselyn, J. A., Kamide, Y., Kroehl , H. W., Rostoker , G., Tsurutani , B. T., Vasyliunas , V. M.: 1994, *Journal of Geophysical Research*, **99**, 5771

Gopalswamy, N., Kaiser, M. L., Thompson, B. J., Burlaga, L. F., Szabo, A., Lara, A., Vourlidas, A., Yashiro, S., Bougeret, J.-L.: 2000, *Geophysical Research Letters* **27**, 1427

Gopalswamy, N., Shimojo, M., Lu, W., Yashiro, S., Shibasaki, K., Howard, R.A.: 2003, *The Astrophysical Journal* **586**, 562

Gopalswamy, N.: 2004a, in: Solar and Space Weather Radiophysics, (eds.) Keller, C. U., Gary, D. E., 305

Gopalswamy, N.: 2004b, in: The Sun and the Heliosphere as an Integrated System, (eds.) Poletto, G., Suess, S. T., Astrophysics and Space Science Library, **317**, 201

Gopalswamy, N.: 2004c, *Planetary and Space Science*, **52**, 1399

Gopalswamy, N., Aguilar–Rodriguez, E., Yashiro, S., Nunes, S., Kaiser, M. L., Howard, R. A.: 2005, *Journal of Geophysical Research*, **110**, A12S07

Gopalswamy, N.: 2006a, *Journal of Astrophysics and Astronomy*, **27**, 243

Gopalswamy, N.: 2006b, in: Solar Eruptions and Energetic Particles, (eds.) Gopalswamy, N., Mewaldt, R., Torsti, J., *AGU, Geophysical Monograph Series*, **165**, 207

Gopalswamy, N., Yashiro, S., Akiyama, S.: 2007, *Journal of Geophysical Research*, **112**, A06112

Gopalswamy, N., Yashiro, S., Akiyama, S., Mäkelä, P., Xie, H., Kaiser, M. L., Howard, R. A., Bougeret, J. L.: 2008, *Annales Geophysicae*, **26**, 3033.

Gopalswamy, N.: 2008, *Journal of Atmospheric and Solar-Terrestrial Physics*, **70**, 2078

Gopalswamy, N., Yashiro, S., Michalek, G., Stenborg, G., Vourlidas, A., Freeland, S., Howard, R.: 2009, *Earth Moon and Planets*, **104**, 295.

Gopalswamy, N., Xie, H., Mäkelä, P., Akiyama, S., Yashiro, S., Kaiser, M. L., Howard, R. A., Bougeret, J. -L.: 2010, *The Astrophysical Journal* **710**, 1111

Gopalswamy, N.: 2010a, in: Solar and Stellar Variability: Impact on Earth and Planets, (eds.) Kosovichev, A. G., Andrei, A. H., Rozelot, J. -P., Proceedings IAU Symposium, **264**, 326

Gopalswamy, N.: 2010b, Proceedings of the 20th National Solar Physics Meeting, Slovakia, 108

Gopalswamy, N., Yashiro, S., Xie, H., Akiyama, S., Mäkelä, P.: 2015, *Journal of Geophysical Research* **120**, 9221

Gosling, J. T., Hildner, E., Macqueen, R. M., Munro, R. H., Poland, A. I., Ross, C. L.: 1974, *Journal of Geophysical Research*, **79**, 4581

Gosling, J. T., Hildner, E., Macqueen, R. M., Munro, R. H., Poland, A. I., Ross, C. L.: 1975, *Solar Physics*, **40**, 439

Gosling, J. T., Hildner, E., MacQueen, R. M., Munro, R. H., Poland, A. I., Ross, C. L.: 1976, *Solar Physics*, **48**, 389

Gosling, J. T.: 1993, *Journal of Geophysical Research*, **98**, 18937

Gosling, J. T.: 1997, in: Coronal Mass Ejections, (eds.) Crooker, N., Joselyn, J. A., Feynman, J., *AGU, Geophysical Monograph Series*, **99**, 9

Gussenhoven, M. S., Mullen., E. G.: 1983, *Journal of Spacecraft and Rockets*, **20**, 26

Harrison, R. A.: 1995, *Astronomy ans Astrophysics*, **304**, 585

Hartz, T. R.: 1964, *Annales d'Astrophysique* **27**, 831.

Hartz, T. R.: 1969, *Planetary and Space Science*, **17**, 267

Hey, J. S., Phillips, J. W., Parsons, S.J.: 1946, *Nature* **157**, 296.

Hildner, E.: 1977, in Study of Travelling Interplanetary Phenomena, (eds.) Shea, M. A., Smart, D. F., Wu, S. T., Astrophysics and Space Science Library, **71**, 3

Hillaris, A., Bouratzis, C., Nindos, A.: 2016, *Solar Physics* **291**, 2049

Ho, G. C., Lario, D., Decker, R. B., Smith, C. W., Hu, Q.: 2008, Particle Acceleration and Transport in the Heliosphere and Beyond, AIP Conference Proceeding 1039, (eds.) Li, G. et al., New York, 184

Howard, R., Sheeley, N. R., Koomen, M. J., Michels, D. J.: 1985, *Journal of Geophysical Research*, **90**, 8173

Hundhausen, A. J., Bame, S. J., Montgomery, M. D.: 1970, *Journal of Geophysical Research*, **75**, 4631

Hundhausen, A. J.: 1993, *Journal of Geophysical Research*, **98**, 13177

Hundhausen, A. J.: 1994, Proceedings of Sixth International Solar Wind Conference, TN306, 181

Hundhausen, A.: 1999, A summary of the results from NASA's solar maximum mission, (eds.) Strong, K. T., Saba, J. L. R., Haisch, B. M., Schmelz, J. T., 143

Huttunen-Heikinmaa, K., Valtonen, E.: 2009, *Annales Geophysicae*, **27**, 767

Hwang, J., Cho, K. S., Moon, Y. J., Kim, R. S., Park, Y. D.: 2010, *Acta Astronautica*, **67**, 353

Illing, R. M. E., Hundhausen, A.J.: 1983, *Journal of Geophysical Research*, **88**, 10210

Isola, C., Favata, F., Micela, G., Hudson, H. S.: 2007, *Astronomy and Astrophysics*, **472**, 261

Ji, E. Y., Moon, Y. J., Gopalswamy, N., Lee, D. H., 2012.: *Journal of Geophysical Research*, **117**, A03209

Jian, L., Russell, C. T., Luhmann, J. G., Skoug, R. M.: 2008, *Advances in Space Research*, **41**, 259

Joshi, B., Manoharan, P. K., Veronig, A. M., Pant, P., Pandey, K.: 2007, *Solar Physics*, **242**, 143.

Jing, J., Yurchyshyn, V. B., Yang, G., Xu, Y., Wang, H.: 2004, *The Astrophysical Journal* **614**, 1054

Kahler, S. W.: 1977, *The Astrophysical Journal*, **214**, 891

Kahler, S., Reames, D. V., Sheeley, N. R., Howard, R. A., Michels, D. J., Koomen, M. J.: 1985, *The Astrophysical Journal*, **290**, 742

Kahler, S. W., Sheeley, N. R., Jr., Liggett, M.: 1989,*The Astrophysical Journal*, **344**, 1026

Kahler, S. W.: 1992, *Annual Review of Astronomy and Astrophysics*, **30**, 113

Kahler, S. W.: 1994,*The Astrophysical Journal*, **428**, 837

Kahler, S. W.: 2001, *Journal of Geophysical Research* **106**, 20947

Kahler, S. W., Reames, D. V.: 2003, *The Astrophysical Journal*, **584**, 1063

Kahler, S. W.: 2006, in: Solar Eruptions and Energetic Particles, (eds.) Gopalswamy, N., Mewaldt, R., Torsti, J., *AGU, Geophysical Monograph Series*, **165**, 21

Kallenrode, M. B.: 2003, *Journal of Physics G: Nuclear and Particle*, **29**, 965

Kang, S. -M., Moon, Y. -J., Cho, K. -S., Kim, Y. -H., Park, Y. D., Baek, J. -H., Chang, H. -Y.: 2006, *Journal of Geophysical Research* **111**, A05102

Kilcik, A., Yurchyshyn, V. B., Abramenko, V., Goode, P. R., Gopalswamy, N., Ozguc, A., Rozelot, J.P.: 2011, *The Astrophysical Journal* **727**, 44

Kim, R. -S., Cho, K. -S., Moon, Y. -J., Kim, Y. -H., Yi, Y., Dryer, M., Bong, S. -C., Park, Y. -D.: 2005, *Journal of Geophysical Research* **110**, A11104

Kim, R. -S., Cho, K. -S., Kim, K. -H., Park, Y. -D., Moon, Y. -J., Yi, Y., Lee, J., Wang, H., Song, H., Dryer, M.: 2008, *The Astrophysical Journal* **677**, 1378

Kim, R. -S., Cho, K. -S., Moon, Y. -J., Dryer, M., Lee, J., Yi, Y., Kim, K. -H., Wang, H., Park, Y. -D., Kim, Y.H.: 2010, *Journal of Geophysical Research*, **115**, A12108

Klein, L. W., Burlaga, L. F.: 1982, *Journal of Geophysical Research*, **87**, 613

Klimchuk, J. A.: 2001, in: Space Weather, (eds.) Song, P., Singer, H., Siscoe, G., *AGU, Geophysical Monograph Series*, **125**, 143

Kocharov, L. G., Kocharov, G. E.: 1984, *Space Science Reviews*, **38** 89

Kocharov, L., Torsti, J. 2002, *Solar Physics*, **207**, 149

Koutchmy, S., Livshits, M.: 1992, *Space Science Reviews*, **61**, 393

Kurt, V., Belov, A., Mavromichalaki, H., Gerontidou, M.: 2004, *Annales Geophysicae*, **22**, 2255

Lam, H. L.: 2009, *Advances in Space Research*, **43**, 1299

Lang, K. R.: 2001, The Cambridge Encyclopedia of the Sun, Cambridge University Press, 268

Lanzerotti L. J.: 2007, Space weather effects on communications, In: Space Weather-Physics and Effects, Springer Praxis Books, Berlin, 247

Lario, D., Hu, Q., Ho, G. C., Decker, R. B., Roelof, E. C., Smith, C. W.: 2005, *Solar Wind 11/SOHO 16, Connecting Sun and Heliosphere*, 81

Le, G. -M., Li, C., Tang, Y. -H., Ding, L. -G., Yin, Z. -Q., Chen, Y. -L., Lu, Y. -P., Chen, M. -H., Li, Z. -Y.: 2016, *Research in Astronomy and Astrophysics* **16**, 14

Le Squeren, A. M. 1963, *Annales d'Astrophysique*, **26**, 97

Lee, J. -O., Moon, Y. -J., Lee, K. -S., Kim, R. -S.: 2014, *Solar Physics*, **289**, 2233

Lee, K., Moon, Y. J., Nakariakov, V. M.: 2016, *The Astrophysical Journal*, **831**, 131

Lin, R. P., Hudson, H. S.: 1976, *Solar Physics*, **50**, 153

Lin, R.P., Anderson, K.A., Ashford, S., Carlson, C., Curtis, D., et al.: 1995, *Space Science Reviews* **71**, 125

Lindsay, G. M., Russell, C. T., Luhmann, J. G., Gazis, P.: 1994, *Journal of Geophysical Research*, **99**, 11

Lindsay, G. M., Russell, C. T., Luhmann, J. G.: 1995, *Journal of Geophysical Research*, **100**, 16999

Loewe, C. A., Prölss, G. W.: 1997, *Journal of Geophysical Research*, **102**, 14209

Lu, Y., Shao, Q., Yue, H., Yang, F.: 2019, *IEEE Access*, **7**, 93473

Mäkelä, P., Gopalswamy, N., Akiyama, S., Xie, H., Yashiro, S.: 2011, *Journal of Geophysical Research*, **116**, A08101

MacQueen, R. M., Fisher, R. R.: 1983, *Solar Physics*, **89**, 89

Mahrous, A., Shaltout, M., Beheary, M. M., Mawad, R., Youssef, M.: 2009, *Advances in Space Research*, **43**, 1032

Malitson, H. H., Fainberg, J., Stone, R. G.: 1973, *Astrophysical Letters*, **14**, 111

Marsden, R. G., Sanderson, T. R., Tranquille, C., Wenzel, K. -P., Smith, E. J.: 1987, *Journal of Geophysical Research*, **92**, 11009

McAllister A. H., Hundhausen, A. J.: 1996, Astronomical Society of the Pacific Conference Series, **95**, 171

McLean, D.J., Labrum, N.R.: 1985, Solar Radiophysics: Studies of Emission from the Sun at Metre Wavelengths.

Mercier, C., Elgaroy, O., Tlamicha, A., Zlobec, P.: 1984, *Solar Physics*, **92**, 375

Meyer, P., Parker, E. N., Simpson, J. A.: 1956, *Physical Review*, **104**, 768

Michałek, G., Gopalswamy, N., Yashiro, S. 2003, *The Astrophysical Journal*, **584**, 472

Michalek, G., Gopalswamy, N., Yashiro, S.: 2007, *Solar Physics*, **246**, 399

Michalek, G.: 2006, *Solar Physics*, **237**, 101

Miller, J. A.: 1998, *Space Science Reviews*, **86**, 79

Miteva, R., Klein, K. L., Samwel, S. W., Nindos, A.,Kouloumvakos, A., Reid, H.: 2013, *Central European Astrophysical Bulletin*, **37**, 541

Moon, Y. -J., Choe, G. S., Wang, H., Park, Y. D., Gopalswamy, N., Yang, G., Yashiro, S.: 2002, *The Astrophysical Journal*, **581**, 694.

Moon, Y. -J., Cho, K. -S., Dryer, M., Kim, Y. -H., Bong, S.-. chan ., Chae, J., Park, Y. D.: 2005, *The Astrophysical Journal*, **624**, 414

Moore, R. L., Sterling, A. C. Hudson, H. S., Lemen, J. R.: 2001, *The Astrophysical Journal*, **552**, 833

Moses, J. D., Ko, Y. -K., Laming, J. M., Provornikova, E. A., Strachan, L., Beltran, S. T.: 2015, *Applied Optics*, **54**, F222

Munro, R. H., Gosling, J. T., Hildner, E., MacQueen, R. M., Poland, A. I., Ross, C.L.: 1979, *Solar Physics*, **61**, 201

Nindos, A., Aurass, H., Klein, K. -L., Trottet, G.: 2008, *Solar Physics*, **253**, 3

Obridko, V. N., Kanonidi, Kh. D., Mitrofanova, T. A., Shelting, B. D.: 2013, *Geomagnetism and Aeronomy*, **53**, 147

Pallavicini, R., Serio, S., Vaiana, G. S.: 1977, *The Astrophysical Journal*, **216**, 108

Papaioannou, A., Sandberg, I., Anastasiadis, A., Kouloumvakos, A., Georgoulis, M. K., Tziotziou, K., Tsiropoula, G., Jiggens, P., Hilgers, A.: 2016, *Journal of Space Weather and Space Climate*, **6**, A42

Park, J., Moon, Y. J., Gopalswamy, N.: 2012, *Journal of Geophysical Research*, **117**, A08108

Payne-Scott, R., Yabsley, D. E., Bolton, J. G.: 1947, *Nature*, **160**, 256

Sturrock, P. A.: 1966, *Physical Review*, **141**, 186

Pick, M.: 2004, Solar and Space Weather Radiophysics, (eds.) Gery, D. E., Keller, C. U., Astrophysics and Space Science Library, **314**, 17

Pirjola, R.: 2007, Space weather effects on power grids. In: Space Weather-Physics and Effects. Springer Praxis Books, Berlin, 269

Pneuman, G. W., Kopp, R. A.: 1971, *Solar Physics*, **18**, 258

Podladchikova, T., Petrukovich, A., Yermolaev, Y.: 2018, *Journal of Space Weather and Space Climate*, **8**, A22

Potter, D. W., Lin, R. P., Anderson, K. A.: 1980, *The Astrophysical Journal*, **236**, L97.

Priest, E. R.: 1982, Solar magnetohydrodynamics, Geophysics and Astrophysics Monographs, Dordrecht, 21

Ramaty, R., Murphy, R. J.: 1987, *Space Science Reviews*, **45**, 213

Raymond, J. C., Thompson, B. J., St. Cyr, O. C., Gopalswamy, N., Kahler, S., Kaiser, M., Lara, A., Ciaravella, A., Romoli, M., O'Neal, R.: 2000, *Geophysical Research Letters*, **27**, 1439

Reames, D. V.: 1990, *The Astrophysical Journal*, **73**, 235

Reames, D. V., Meyer, J. P., von Rosenvinge, T. T.: 1994, *The Astrophysical Journal Supplement Series*, **90**, 649

Reames, D. V.: 1995, *Advances in Space Research*, **15**, 41

Reames, D. V., Barbier, L. M., Ng, C. K.: 1996, *The Astrophysical Journal*, **466**, 473

Reames, D. V.: 1999, *Space Science Reviews*, **90**, 413

Reames, D. V.: 2013, *Space Science Review*, **175**, 53

Reiner, M. J., Vourlidas, A., Cyr, O. C. S., Burkepile, J. T., Howard, R. A., Kaiser, M. L., Prestage, N. P., Bougeret, J. -L.: 2003, *The Astrophysical Journal*, **590**, 533

Richardson, I. G., Cane, H. V.: 2010, *Solar Physics*, **264**, 189

Richardson, I. G., Cane, H. V.: 2012, *Journal of Space Weather and Space Climate*, **2**, A01

Richardson, I. G., Webb, D. F., Zhang, J., Berdichevsky, D. B., Biesecker, D. A., Kasper, J. C., Kataoka, R., Steinberg, J. T., Thompson, B. J., Wu, C. -C., Zhukov, A. N.: 2006, *Journal of Geophysical Research* **111**, A07S09

Richardson, I. G., von Rosenvinge, T. T., Cane, H. V., Christian, E. R., Cohen, C. M. S., Labrador, A. W., Leske, R. A., Mewaldt, R. A., Wiedenbeck, M. E., Stone, E. C.: 2014, *Solar Physics*, **289**, 3059

Richter, A. K., Hsieh, K. C., Luttrell, A. H., et al.: 1985, in: Collisionless Shocks in the Heliosphere: Reviews of Current Research, (eds.) Tsurutani, B. T., Stone, R. G., *AGU, Geophysical Monograph Series*, **35**, 33

Rosenberg, R. L., Coleman, J. P. J.: 1980, *Journal of Geophysical Research*, **85**, 3021

Roussev, Ilia I., Sokolov, Igor V.: 2006, in: Solar Eruptions and Energetic Particles, (eds.) Gopalswamy, N., Mewaldt, R., Torsti, *AGU, Geophysical Monograph Series*, **165**, 89

Roussev, I. I., Sokolov, I. V., Forbes, T. G., Gombosi, T. I., Lee, M. A., Sakai, J. I.: 2004, *The Astrophysical Journal*, **605**, L73

Russell, C. T.: 2001, in: space Weather, (eds.) Paul, S., Howard J. S., George L. S., *AGU, Geophysical Monograph Series*, **125**, 73

Rust, D. M, Hildner, E., Hansen, R. T., Dryer, M., McClymont, A. N., et al.: 1980, (ed.) Sturrock, P. A., Skylab Solar Workshop II, 273

Salas-Matamoros, C., Klein, K. -L.: 2015, *Solar Physics*, **290**, 1337

Sarris, E. T., Van Allen, J. A.: 1974, *Journal of Geophysical research*, **79**, 4157

Schmieder, B., Démoulin, P., Aulanier, G.: 2013, *Advances in Space Research*, **51**, 1967

Shanmugaraju, A., Moon, Y. J., Vrsnak, B.: 2011, *Solar Physics*, **270**, 273

Shanmugaraju, A., Syed Ibrahim, M., Moon, Y. -J., Mujiber Rahman, A., Umapathy, S.: 2015, *Solar Physics*, **290**, 1417

Sheeley, N. R. Jr, Bohlin, J. D., Brueckner, G. E., Purcell, J. D., Scherrer, V. E., et al.: 1975, *Solar Physics* **45**, 377

Sheeley, N. R. Jr, Harvey, J. W., Feldman, W. C.: 1976, *Solar Physics*, **49**, 271

Sheeley, N. R. Jr., Howard, R. A., Koomen, M. J., Michels, D. J.: 1983, *The Astrophysical Journal*, **272**, 349

Sheeley, N. R. Jr., Howard, R. A., Michels, D. J.: 1984, *The Astrophysical Journal*, **279**, 839

Sheeley, N. R. Jr., Howard, R. A., Michels, D. J., Koomen, M. J., Schwenn, R., Muehlhaeuser, K. H., Rosenbauer, H.: 1985, *Journal of Geophysical Research* **90**, 163

Sheeley, N. R. Jr., Walters, J. H., Wang, Y. M., Howard, R. A.: 1999, *Journal of Geophysical Research*, **104**, 24739

Shen, C. L., Liao, C. J., Wang, Y. M., Ye, P. Z., Wang, S.: 2013, *Solar Physics*, **282**, 543

Smith, E. J., Wolf, J. H.: 1976, *Geophysical Research Letters*, **3**, 137

Smith, Z., Murtagh, W., Smithtro, C.: 2004, *Journal of Geophysical Research*, **109**, A01110

Srivastava, N., Venkatakrishnan, P.: 2004, *Journal of Geophysical Research*, **109**, A10103

St Cyr, O. C., Webb, D. F.: 1991, *Solar Physics*, **136**, 379

Sterling, A. C., Moore, R. L., Freeland, S. L.: 2011, *The Astrophysical Journal*, **731**, L3

Subramanian, P., Dere, K. P., Rich, N. B., Howard, R. A.: 1999, *Journal of Geophysical Research*, **104**, 22321

Sugiura, M.: 1964, *Annals of the International Geophysical Year*, **35**, 9

Szajko, N. S., Cristiani, G., Mandrini, C. H., Dal Lago, A.: 2013, *Advances in Space Research*, **51**, 1842

Tang, J. F., Wu, D. J., Tan, C. M.: 2013, *The Astrophysical Journal*, **779**, 83

Temerin, M., Li, X.: 2002, *Journal of Geophysical Research*, **107**, 1472

Temerin, M., Li, X.: 2006, *Journal of Geophysical Research*, **111**, A04221

Torsti, J., Valtonen, E., Lumme, M., Peltonen, P., Eronen, T., et al.: 1995, *Solar Physics*, **162**, 505

Tsurutaini B. T., Gonzalez, W. D.: 1997, in: Magnetic Storms, (eds.) Bruce, T. T., Walter, D. G., et al., *AGU, Geophysical Monograph Series*, **98**, 77

Tsurutani, B. T., Lakhina, G. S., Hajra, R.: 2019, EGU, Nonlinear Processes in Geophysics (in press)

Valtonen, E., Laitinen, T., Huttunen-Heikinmaa, K.: 2005, *Advances in Space Research*, **36**, 2295

Valtonen, E.: 2004, Lecture Notes in Physics, Berlin Springer Verlag, **656**, 241

Vasanth, V., Umapathy, S.: 2013, *ISRN Astronomy and Astrophysics*, **2013**, 129426

Vršnak, B, Marišić, D., Stanger, A. L., Veronig, A.: 2004, *Solar Physics*, **225**, 355

Vršnak, B., Sudar, D. Ruždjak, D.: 2005, *Astronomy and Astrophysics*, **435**, 1149

Vršnak, B., Žic, T., Vrbanec, D., Temmer, M., Rollett, T., et al.: 2013, *Solar Physics*, **285**, 295

Wagner, W. J., MacQueen, R. M.: 1983,*Astronomy and Astrophysics*, **120**, 136

Wang, Y. M., Ye, P. Z., Wang, S., Zhou, G. P., Wang, J. X.: 2002, *Journal of Geophysical Research*, **107**, 1340

Wang, R.: 2006, *Astroparticle Physics*, **26**, 202

Webb, D. F., Hundhausen, A. J.: 1987, *Solar Physics*, **108**, 383

Webb, D. F., Cliver, E. W., Crooker, N. U., Cry, O. C. S., Thompson, B.J.: 2000, *Journal of Geophysical Research*, **105**, 7491.

Webb, D. F., Howard, R. A.: 1994, *Journal of Geophysical Research*, **99**, 4201

Weiss, A. A., Stewart, R. T.: 1965, *Australian Journal of Physics*, **18**, 143

Whang, Y. C.: 1988, *Journal of Geophysical Research*, **93**, 5897

Wik, M., Viljanen, A., Pirjola, R., Pulkkinen, A., Wintoft, P., Lundstedt, H.: 2008, *Space Weather*, **6**, 07005

Wild, J. P., McCready, L. L.: 1950, *Australian Journal of Scientific Research*, **3**, 387

Wild, J. P., Smerd, S. F.: 1972, *Annual Review of Astronomy and Astrophysics*, **10**, 159

Wild, J. P., Murray, J. D., Rowe, W. C.: 1954, *Australian Journal of Physics*, **A7**, 439

Wild, J. P., Sheridan, K. V., Trent, G. H. 1959a, The transverse motions of the sources of solar radio bursts, in: Paris Symposium on Solar Radio Astronomy, (eds.) Bracewell, R. N., Stanford University Press, Stanford, 176

Wild, J. P., Sheridan, K. V., Neylan, A. A.: 1959b, *Australian Journal of Physics*, **12**, 369

Wu, C. S., Wang, C. B., Yoon, P. H., Zheng, H. N., Wang, S.: 2002, *The Astrophysical Journal*, **575**, 1094

Xu, D., Chen, T., Zhang, X. X., Liu, Z.: 2009, *Planetary and Space Science*, **57**, 1500

Yakovchouk, O. S., Mursula, K., Holappa, L., Veselovsky, I.S., Karinen, A.: 2012, *Journal of Geophysical Research*, **117**, A03201

Yashiro, S., Gopalswamy, N., Michalek, G., St. Cyr, O. C., Plunkett, S. P., Rich, N. B., Howard, R. A.: 2004, *Journal of Geophysical Research*, **109**, A07105.

Yashiro, S., Akiyama, S., Gopalswamy, N., Howard, R.: 2006, *The Astrophysical Journal Letters*, **650**, L143

Youssef, M.: 2012, *NRIAG Journal of Astronomy and Geophysics*, **1**, 172

Yurchyshyn, V., Karlický, M., Hu, Q., Wang, H.: 2006, *Solar Physics*, **235**, 147

Zhang, J., Dere, K. P., Howard, R. A., Kundu, M. R., White, S. M.: 2001, *The Astrophysical Journal*, **559**, 452

Zhang, J., Dere, K. P., Howard, R. A., Bothmer, V.: 2003, *The Astrophysical Journal*, **582**, 520

Zhang, J., Dere, K. P., Howard, R. A., Vourlidas, A.: 2004, *The Astrophysical Journal*, **604**, 420

Zhang, J., Dere, K. P.: 2006, *The Astrophysical Journal*, **649**, 1100

Zhang, J., Richardson, I. G., Webb, D. F., Gopalswamy, N., Huttunen, E., et al.: 2007, *Journal of Geophysical Research*, **112**, A10102.

Zhang, M., Golub, L., DeLuca, E., Burkepile, J.: 2002, *The Astrophysical Journal*, **574**, L97

Zhang, M., Golub, L.: 2003, *The Astrophysical Journal*, **595**, 1251

Zhang, X. Y., Moldwin, M. B.: 2014, *Journal of Geophysical Research*, **119**, 658

Zhao, X. P., Webb, D. F.: 2003, *Journal of Geophysical Research*, **108**, 1234

UNIVERSITY OF TURKU

Painosalama Oy, Turku, Finland 2019

ISBN 978-951-29-7913-4 (PRINT)
ISBN 978-951-29-7914-1 (PDF)
ISSN 0082-7002 (Print)
ISSN 2343-3175 (Online)